Hydrodynamic characterization of
a Denver laboratory flotation cell

Sung-Su Do

Department of Mining, Metals and Materials Engineering

McGill University

Montreal, Canada

A thesis submitted to the Faculty of Graduate Studies and Research in partial fulfillment of the requirements for the degree of Master of Engineering

Advisors:

Dr. J.A. Finch

Dr. C.O. Gomez

Canada

This thesis is dedicated to God who has saved me from

my sins and given me new meaning of life,

to my wife Seon-Mi Ha,

and my daughter Mary-Joy Do

Abstract

Gas dispersion in a laboratory Denver flotation cell was characterized by measuring the superficial gas velocity (J_g), bubble size (d_b) and estimating the bubble surface area flux, S_b as a function of impeller speed, frother concentration (Dowfroth 250), and solids content (-30μm silica). The cell was operated by self-aspiration or forced air. The air flow rate was measured using a McMillan meter (self-aspiration) and a mass flow meter (forced air). The bubble size was measured by a photographic technique developed at McGill. From repeat experiments, the average relative standard deviation on J_g was ca. 2% and on d_b was ca. 13%. No effect of location on bubble size was found.

In self-aspiration mode J_g increased with impeller speed due to increased suction and decreased with increasing frother concentration and solids content. The effect of frother was attributed to increased recirculation of air as the bubble size was reduced. The effect of solids appears related to sedimentation. Bubble size increased with increasing impeller speed, which was attributed to the increase in J_g. Solids did not affect the bubble size. Bubble size decreased with frother most notably at low concentration then remained almost constant at high frother concentration. The critical coalescence concentration appeared to be close to 5 ppm for the present conditions. The bubble surface area flux S_b increased approximately linearly with impeller speed up to ca. $40s^{-1}$.

Using forced air the bubble size behaved as expected: it decreased with increasing impeller speed (due to higher shear) and decreasing J_g. The S_b ranged up to ca. $80s^{-1}$, higher than values quoted for a laboratory machine. To correspond more closely to industrial cells, operation with forced air is recommended. The use of higher impeller speeds than are commonly used in laboratory testwork will give more closely fit superficial gas velocity found in industrial plant practice.

Résumé

La caractérisation de la dispersion du gaz dans une cellule de flottation en laboratoire de type Denver fut effectuée en mesurant la vélocité superficielle du gaz (J_g), la dimension de bulles (d_b) et en estimant le flux de superficie des bulles, S_b, par rapport à la vitesse de la roue à aubes, la concentration de moussant (Dowfroth 250), et du contenu de solides (silice, -30 µm). La cellule fut opérée avec air auto-aspiré ou forcé. Le débit d'air fut mesuré à l'aide d'un débitmètre McMillan (auto-aspiration) ou un débitmètre de masse (air forcé). La dimension des bulles fut déterminée à l'aide d'une technique photographique développée à McGill. Des tests répétés ont démontré un écart type relatif moyen d'environ 2% pour le J_g et de 13% pour d_b. La localisation de l'échantillonnage n'avait aucun effet sur la détermination de la dimension des bulles.

En mode auto-aspiration, le J_g augmenta avec la vitesse de la roue à aubes à cause de l'augmentation de la succion et diminua avec une augmentation de moussant ou du contenu de solides. L'effet du moussant est attribué à l'augmentation de la recirculation de l'air dû à la diminution de la dimension des bulles. L'effet des solides semble connexe à la sédimentation. L'augmentation de la dimension des bulles avec la vitesse de la roue à aubes fut attribuée à la hausse en J_g. Le contenu de solides n'a pas eu d'effet sur la dimension des bulles. L'ajout de moussant, surtout à basse concentration, diminua la dimension des bulles pour atteindre un plateau à haute concentration. Le point de concentration critique à la coalescence se situe près de 5 ppm pour les conditions actuelles. Le flux de la superficie des bulles, S_b, augmenta presque linéairement avec la vitesse de la roue à aubes jusqu'à environ 40 s^{-1}.

Lorsqu'un débit d'air forcé fut utilisé, la dimension des bulles se comporta tel que prévu : elle diminua avec une augmentation de la vitesse de la roue à aubes (en raison du cisaillement plus élevé). Le flux de la superficie des bulles atteignit environ 80 s^{-1}, une valeur plus élevée que présentement rapporté pour les

cellules de flottation en laboratoire. En utilisant l'air forcé et une vitesse de la roue à aubes plus grande que normalement utilisée en laboratoire, la vélocité superficielle du gaz et le régime opérationnel pourront s'apparenter à ce qui est observé en pratique industrielle.

Acknowledgements

Table of contents

List of figures

Lists of tables

Chapter 1. Introduction

1.1 Background

1.1.1 Flotation

Froth flotation, or simply flotation, was developed in the early 20th century originally for the separation of minerals from ores. It is still the most efficient and widely used method for mineral concentration with an estimated two billion tonnes of ore treated each year (Brewis, 1991; Brewis, 1996). It is used for almost all sulfide minerals and many nonsulfide metallic minerals, industrial minerals, and energy minerals (coal, bitumen). The process has now extended to other industrial fields such as the removal of solids from wastewater, in de-inking recycled paper, the removal of organic contaminants from effluents in the milk and beer industry and remediation of contaminated soil, etc (Brewis, 1991).
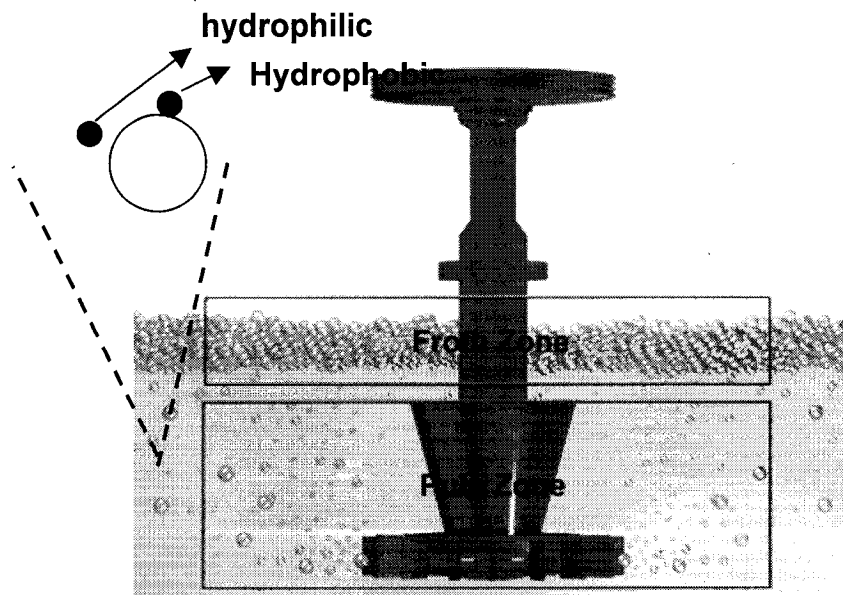
Figure 1. Principle of froth flotation

Flotation is based on the concept that hydrophobic particles suspended in an aqueous phase tend to attach to introduced air bubbles, forming bubble-particle aggregates. The bubbles then carry the hydrophobic particles to the surface of the pulp phase where a stable froth forms. The froth is removed, and the minerals recovered. The unattached hydrophilic particles remain in the pulp, and are either discarded or reprocessed separately. Chemicals are added to control particle hydrophobicity and promote bubble dispersion and froth formation. Figure 1 shows the principle of froth flotation. The process utilizes the natural or induced differences in physico-chemical surface properties of particles of various minerals. The process is applied to relatively fine particles ($<500\mu m$) with some exception such as potash flotation where particles over 2 mm are treated.

Before flotation can be carried out, crushing and grinding must liberate the minerals. The ground material is conditioned with flotation reagents, which may include collectors, frothers, activators and other surface modifying agents. The role of collectors is to form a hydrophobic surface film on the mineral, and thus makes it susceptible to capture by air bubbles. Frothers are used to reduce bubble size and form a stable froth phase on the surface of pulp.

1.1.2 Flotation variables

Flotation involves many variables. Klimpel et al. (1986) suggested flotation as an interactive system of chemical, operational and machine factors.

Chemical factors

Collectors
Frothers
Depressants/Activators
pH, Eh, Water chemistry
Aggregation

Interactive
flotation system

Machine factors

Operational factors

Impeller speed Air flow rate Froth depth Cell design Impeller/stator desian	Ore type Cell residence time Particle size Pulp density Temnerature
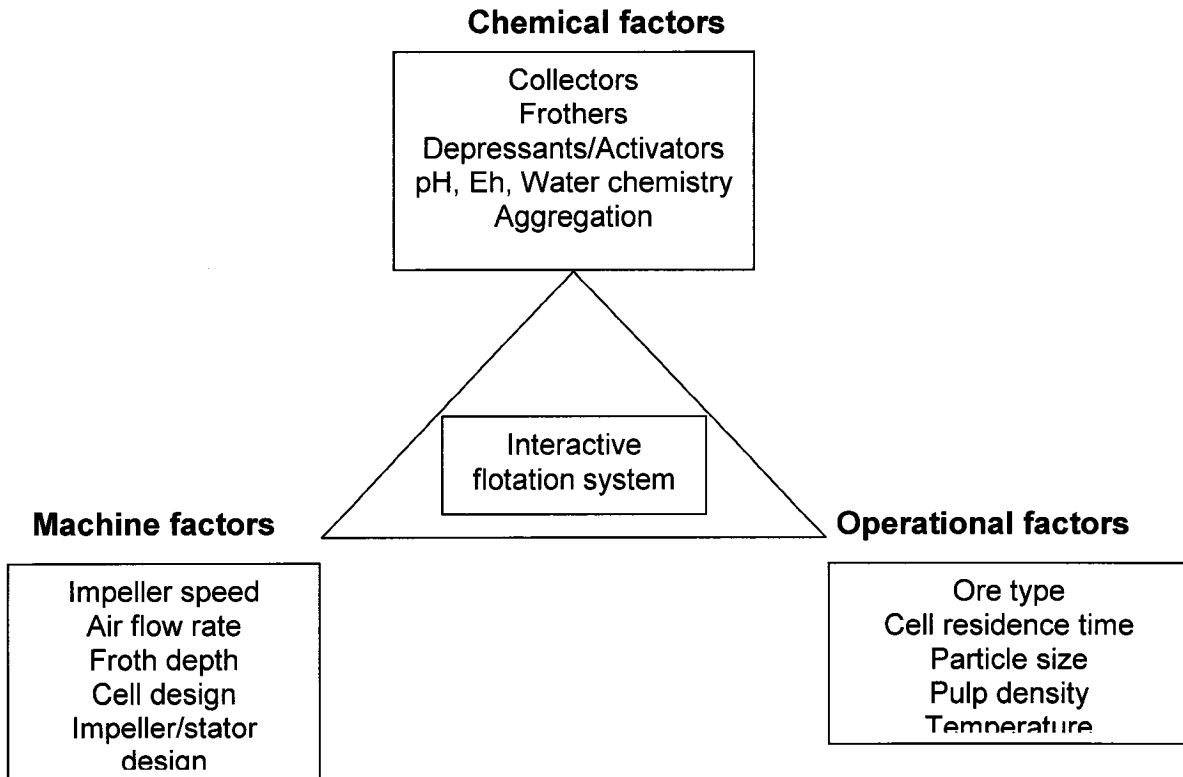
Figure 2. Summary of main process variables (Klimpel et al, 1995)

The overall flotation rate constant k is considered to be a function of these three factors summarised by (Gorain et al., 1997):

$$k = P \ S_b \ R_f \qquad (1.1)$$

where P, the particle floatability, represents the chemical factor, R_f, froth recovery factor, is an operational parameter, and S_b, the bubble surface area flux, is the machine factor.

1.1.3 Machine variables

The role of machine variables has received less attention than the chemistry even though it is a fundamental aspect of flotation. Recently, the interest has increased. The representative machine variables are impeller speed, air flow rate and cell geometry. Some of the early work tried to relate dimensionless groups

15

such as Reynolds number, Froude number, Power number, Air Flow number and Weber number to the metallurgical (grade, recovery) performance. The dimensionless numbers were used to quantify the effect of different machine factors on flotation performance. Table 1 shows examples of dimensionless groups.

Table 1: Dimensionless groups used to characterize flotation cell hydrodynamics (from Gorain, 1996)

Group	Definition	Range
Reynolds number	$Re = \rho_f ND^2 / \mu$	$10^6 - 7 \times 10^6$
Froude number	$F_r = DN^2 / g$	0.1-5
Power number	$N_p = P_0 / \rho_f N^3 D^5$	0.5-5
Air Flow number	$Q_L = Q / ND^3$	0.01-0.2
Modified air flow number	$Q_{ML} = Q / AND$	$10^{-3} - 3 \times 10^{-3}$
Weber number	$We = \rho_f N^2 D^3 / S$	

N= impeller speed, D=impeller diameter, Q=Volumetric air flow rate

P_0= net power input, ρ_f= slurry density, g = gravitational constant, S= surface tension, A=cross sectional area of cell, μ=slurry viscosity

These dimensionless groups have shown generally limited correlation with metallurgical performance. Cell manufacturers emphasise different aspects and there is no agreement to correlate these numbers to flotation cell design and scale-up. This could be because the machine factors do not influence metallurgy directly but create hydrodynamic conditions (solid suspension, gas dispersion and bubble-particle interaction) in the cell and these conditions in turn affect the metallurgical performance. This concept is shown in Figure 3.

```
┌─────────────────────────────────┐
│ Hydrodynamic conditions         │
└─────────────────────────────────┘

┌──────────────┐    ┌──────────────────────────┐    ┌──────────────┐
│ Impeller speed│    │ Solids suspension        │    │ Metallurgical│
│ Air flow rate │ ─► │ Gas dispersion           │ ─► │ performance  │
│ Cell design   │    │ Bubble-particle interaction│   │              │
└──────────────┘    └──────────────────────────┘    └──────────────┘
```
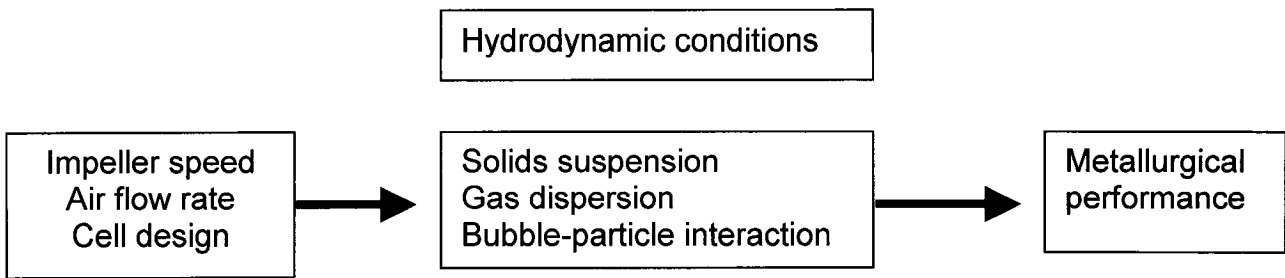
Figure 3. Relating machine operating variables, cell hydrodynamic conditions and metallurgical performance (from thesis of Gorain, B.K. 1996)

Among the hydrodynamic parameters, gas dispersion is considered the key one. Three measures of gas dispersion are gas rate, bubble size, and gas holdup, along with the derived parameter, bubble surface area flux. Pursuing this notion, Gorain et al. (1996) found that the flotation rate constant was not readily related to bubble size, gas holdup or gas rate individually, but it was related to bubble surface area flux, (which is defined as the surface area of bubbles per unit time per unit cross-sectional area of a flotation cell. The unit is: (m^2 bubble surface/s)/(m^2 cell) or s^{-1}).

1.1.4 Flotation machines

Industrial flotation machines may be divided into four classes (Brewis, 1991; Brewis, 1996; Young, 1982):

1. Mechanical:
2. Pneumatic;
3. Froth separators
4. Columns

Pneumatic and froth separation devices are not common in industry today. Columns became important during the 80's but the mechanical cell remains the dominant machine. The mechanical cell is so-named because of the impeller used to suspend particles and generate and disperse bubbles. The generation of

bubbles is achieved by the rotation of the impeller. Air introduced into the impeller region accumulates in the low pressure region behind the impeller blades. This air pocket moves with the blade and is sheared into bubbles along its outer edge (or surface) due to the high velocity relative to the slurry. Even though the impeller assembly and the vessel shape may be different for the various cells, the basic aim remains the same: to keep the solids suspended, disperse the gas as bubbles, provide the hydrodynamic conditions for bubble-particle aggregates to form and to transport collected particles to the froth phase.

The current design of flotation column, developed from an invention in Canada in the early 1960's, experienced rapid growth over the past two decades. It is suitable for fine particle flotation due to its high selectivity. The flotation column has no impeller, instead using a variety of bubble generation systems and often employs wash water added into the top of the froth to help remove entrained contaminants. The bubble generation systems include: forcing air through porous material (perforated rubber, filter cloth or, in the laboratory, sintered metal powder), by shear over an in-line mixer, or by introducing the air as a high velocity jet.

1.1.5 Laboratory flotation testing

Development of a flotation process for a specific ore relies heavily on laboratory testwork. Such testing is also carried out on samples from existing plants to guide full-scale operation. The bulk of laboratory testwork is carried out in batch flotation cells. The two most important requirements of laboratory machines are reproducibility and a metallurgical performance that can be related to commercial operation.

1.1.5.1 Denver laboratory flotation cell

Probably the most widely used is the Denver laboratory flotation cell. The cells are mechanically agitated, and they simulate the large-scale models

18

commercially available. Introduction of air is normally via a hollow standpipe surrounding the impeller shaft. The action of the impeller draws air down the standpipe (i.e., the machine self aspirates), the air rate being controlled by the speed of the impeller. The set-up can be modified for "forced" air injection. Either way, the air stream is sheared into fine bubbles by the impeller.
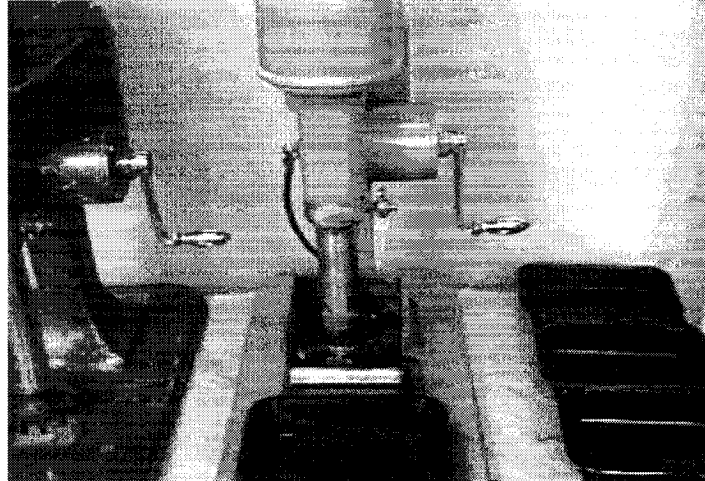
Figure 4. Laboratory flotation cell

1.2 Research objectives

The thesis aims to characterize a laboratory flotation cell by estimating bubble surface area flux, S_b. The use of S_b is restrained by the need to estimate bubble size, d_b. The McGill Mineral Processing group has developed a photographic technique to measure d_b, which can be used in flotation systems (i.e., in the presence of solids). The effect of operating variables such as impeller speed, air flow rate, frother concentration and solids content on bubble size, superficial gas velocity and bubble surface area flux were investigated in a Denver type cell using both aspirated and forced air. The specific objectives are:

1. To determine superficial gas velocity and bubble size as a function of the operating variables (impeller speed, frother concentration and solids content) using aspirated air and forced air;

19

2. To estimate bubble surface area flux as a function of operating variables using aspirated air and forced air.

Chapter 2. Literature review

2.1 Bubble surface area flux (S_b)

2.1.1 Definition of S_b

Bubble surface area flux is defined as the surface area of bubbles per unit time per unit cross-sectional area of a flotation cell. The unit is: (m^2 bubble surface/s)/(m^2 cell) or s^{-1}. The concept is illustrated in Figure 5: air being aspirated down the standpipe by rotation of impeller or forced by pushing air through mass flow meter, Q_g (m^3/s) is divided by some bubble generating device into n bubbles each of surface area $S(m^2)$ and they pass through cell area $A(m^2)$.
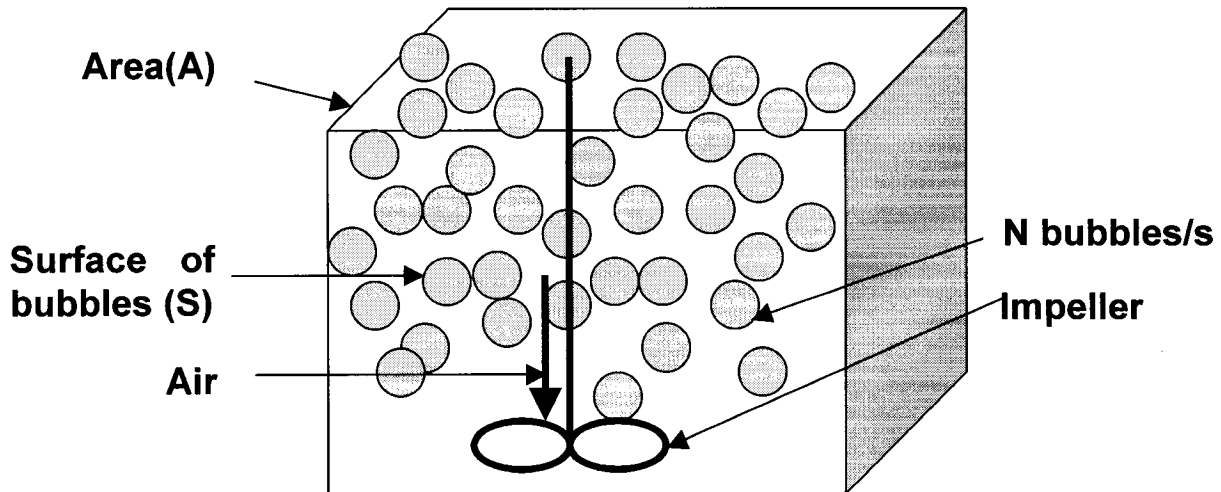
Figure 5. Illustration of bubble surface area flux concept (Finch et al., 1999)

By definition, the bubble surface area flux is given by:

$$S_b = \frac{NS}{A} \tag{2.1}$$

If we assume equal sized spherical bubbles, we can substitute for n ($=6Q_g/\Pi d_b^3$) and S ($=\Pi d_b^2$) to give

21

$$S_b = \frac{6J_g}{d_bA} \qquad (2.2)$$

Since by definition the superficial gas velocity, $J_g = Q_g/A$, then

$$S_b = \frac{6J_g}{d_b} \qquad (2.3)$$

In practice d_b is usually estimated by the Sauter mean diameter.

.

2.1.2 Relevance of S_b

Jameson et al. (1977), and Ahmed and Jameson (1985) derived that the flotation rate constant was given by $k = 1.5\ E_cJ_g/d_b$ where E_c is the collection efficiency. This can be re-written in terms of S_b as $k = 0.25E_cS_b$, which, by comparison, means $P = 0.25E_c$.

The three major measured gas dispersion parameters are bubble size, gas holdup and superficial gas velocity. The importance of bubble size in flotation has been understood since the early days. Smaller bubbles deliver a higher flotation rate constant irrespective of the material. But the finding is true only for a given air flow rate. At different air flow rates, bubble size by itself is not expected to describe the impact on performance.

Gas holdup reflects both gas rate and bubble size and may be expected to better correlate with metallurgy than either alone (Finch et al., 2000).

The rate constant increases with superficial gas velocity up to a certain value but then decreases for high air flow rate (Laplante et al., 1983a; Dobby and Finch,

1990). Any trend will be obscured by significant changes in bubble size, as expected when gas rate is varied.

Gorain et al. (1997) conducted experiments designed to reveal the relationship between the flotation rate constant and various gas dispersion parameters. They concluded that the flotation rate constant is best correlated with the bubble surface area flux.

Figure 6 shows an example of their findings. The plots show a linear relationship between k and S_b for the four impellers. They concluded S_b was independent of impeller type, suggesting that S_b is the key machine variable.
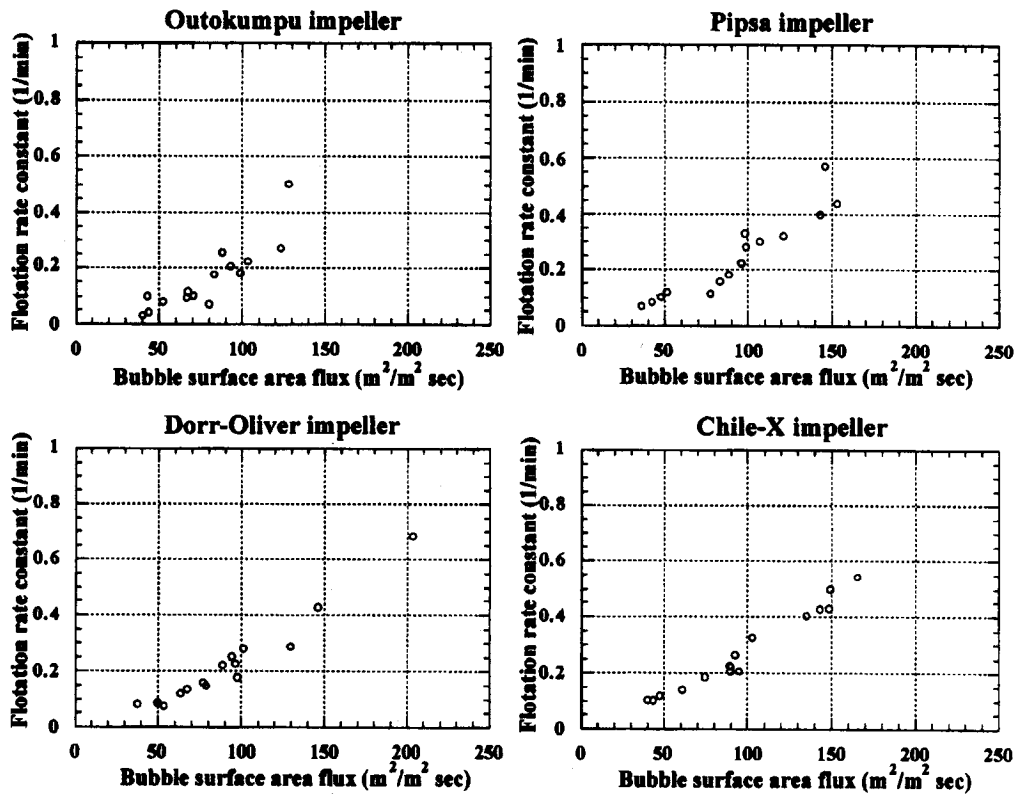
Figure 6. Flotation rate constant as a function of bubble surface area flux for four different impellers (from Gorain et al., 1997)

2.2 Flotation kinetics

2.2.1 Plug flow

One extreme of mixing is plug flow where the residence time of all elements of the fluid (and all particles) is the same.

A batch system with zero order kinetics yields a concentration (C(t)) which decreases linearly down to zero, at a time equal to C(0)/k:

from an initial, time 0, value, C(0),

$$C(t) = C(0)\text{-kt, or 1-kt (dimensionless)} \qquad (2.4)$$

The units of k are g/L/s, or when mass rather than concentration is used, g/s (dM/dt =-k).

But zero order systems are rarely encountered. More common are those in which the reaction proceeds at a rate proportional to the concentration of reacting species (i.e., first order). This assumption is widely applied to flotation systems. The corresponding rate equation for a batch flotation process may be written as follows:

$$-dC/dt = kC \qquad (2.5)$$

where C is the concentration of particles with identical flotation properties in the pulp and t is time. Integrating,

$$\int_{C(0)}^{C(t)} \frac{dC}{C} = -k \int_0^t dt \qquad (2.6)$$

$$\ln \frac{C(t)}{C(0)} = -kt \qquad (2.7)$$

where $C(t)$ = mass fraction at time t, and $C(0)$ = mass fraction at t=0

that is,

$$C(t) = C(0) \exp(-kt) \qquad (2.8)$$

since unreacted mass is $C(t)/C(0)$

then fractional recovery R is given by

$$R = 1 - C(t)/C(0) = 1 - \exp(-kt) \qquad (2.9)$$

2.2.2 Perfectly mixed flow

The other extreme is a perfectly mixed reactor where there is a distribution of retention time and where the concentration is the same throughout the reactor. For a system exhibiting perfect mixing with a mean residence time τ, fractional recovery is given by

$$R = 1 - (1 + k\tau)^{-1} \qquad (2.10)$$

A first order reaction in a perfectly mixed reactor after n reactors yields:

$$R = 1 - \frac{1}{(k\tau + 1)^n} \qquad (2.11)$$

2.3 Hydrodynamics of laboratory flotation cell

Researchers, notably at Columbia University, performed studies to elucidate the contribution of cell hydrodynamics to flotation by Arbiter et al., (1964,1968,1969), Arbiter and Steininger (1965), Harris et al., (1983) and Harris and Khandrika (1984a,b, 1985a,b,c). An aspect they studied was the power consumption.

25

The variables considered included: tank diameter (T), impeller diameter (D), liquid depth (H), distance of impeller above the bottom (C), length (L), and width (W), of impeller blades, width of baffles or shrouding (J) and size of solid particles (d). Flotation systems were described by dimensionless groups: power number, N_p, Reynolds number, N_{Re}, and air flow number, N_Q (see Table 1).

The total flow through an impeller and its associated shrouding involves three constituents: (a) liquid, (b) air directly introduced to the impeller from outside the system, and (c) re-circulated air from the air-liquid mixture in the vessel. Oyama and Endoh (1955) found that the air-liquid composite density in the zone surrounding the impeller is lower than that of the rest of the cell. Several reasons can be proposed. The fact that air flows radially outwards from the impeller leads to a diminishing air concentration gradient with distance from the impeller. Another mechanism, air re-entrainment, occurs with all impeller designs and particularly with flotation impeller-shroud systems.

For mixers operating in the fully turbulent region regime with no vortexing, the power consumption is directly proportional to the liquid density:

$$P_L = N_P \rho_L N^3 D^5 \qquad (2.12)$$

where P_L=power consumption in the liquid, N_p=power number, ρ_L=density of liquid, N=impeller speed, D=impeller diameter

2.3.1 Liquid-Air system

2.3.1.1 Power

Figure 7 illustrates the power ratio-air flow number correlation for two laboratory flotation machines. The power ratio P_{AL}/P_L is the power consumption in aerated liquid (P_{AL}) to the power consumption in liquid only (P_L). It was found in all cases that the power ratio decreased as N_Q increased.
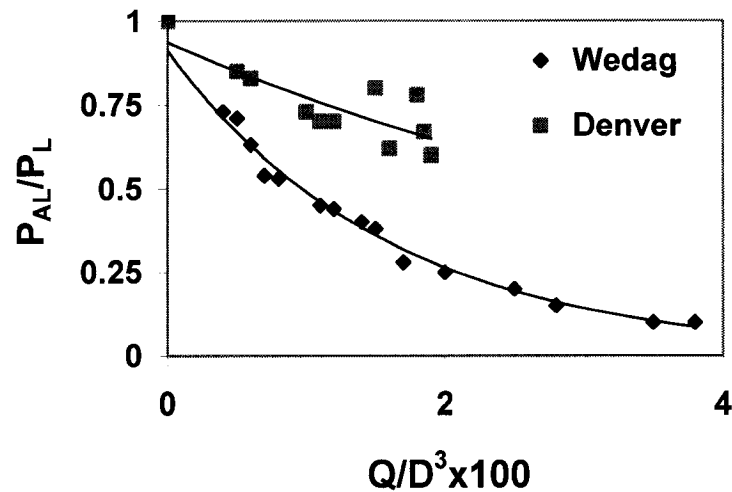
Figure 7. Power ratio as a function of air flow numbers (redrawn from Arbiter and Steininger, 1965)

From the work of Oyama and Endoh (1955) the decrease in the power consumption in air-liquid systems is due to the lower density of the air-liquid mixture. However, the power number calculated from the apparent density of the composite mixture was found to be higher than expected if the air were evenly dispersed throughout the system. Arbiter et al. (1964) concluded that the air-liquid mixture in the vessel was not homogeneous, and in particular that the density in the zone around the impeller was lower than overall average density.

2.3.1.2 Cell design and operating factors

The air aspirated naturally by a self-aeration machine depends upon several factors. Figure 8 shows air flow rate as a function of impeller speed for different impeller submergence. At a fixed speed, increasing the impeller submergence leads to increased aeration rate (Figure 8). This is a hydrostatic effect.
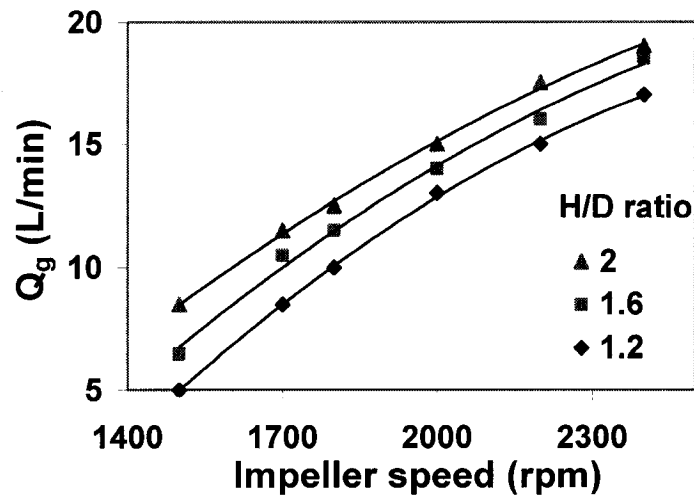
Figure 8. Air flow rate as a function of impeller speed for different impeller submergence, H/D (where H: liquid depth, D: impeller diameter): Fagergren lab cell (redrawn from Arbiter et al., 1968).

Figure 9 shows air flow rate as a function of impeller speed for different T/D ratio (the ratio between tank diameter (T) and impeller diameter (D)). Increasing T/D increases aeration rate. The effect of increasing T/D is attributed to a lower proportion of fresh air being drawn in because more air is being recirculated in the larger tank.
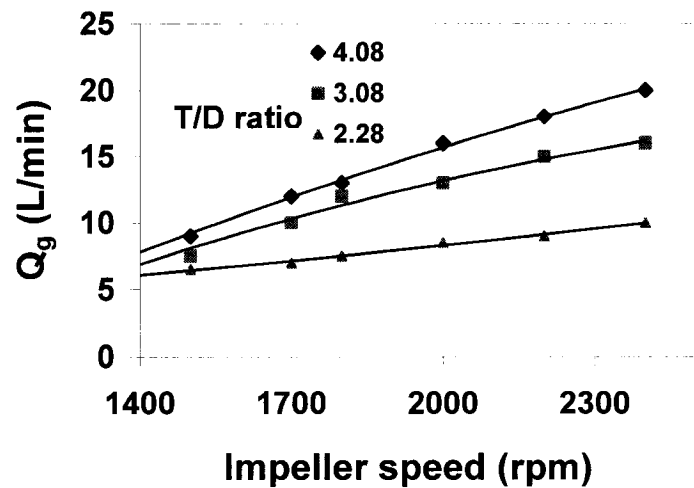
Figure 9. Air flow rate as a function of impeller speed for different T/D ratio: Fagergren lab cell (redrawn from Arbiter et al., 1968)

Another factor studied was the design of the impeller blades. In two Agitair cells the impellers differed in that one had rounded posts while the other had wedge posts: The latter had twice the power number.

Figures 8 and 9 show that increasing impeller speed increases the rate of aspiration of air. This is attributed to the suction generated by the impeller increasing with increasing impeller speed: (suction α (impeller speed)^2) (Harris and Khandrika. 1985b).

2.3.1.3 The effect of frother

Figure 10 shows that the power consumption decreases when frother is added. A decrease in power consumption for increasing frother concentration can be attributed to partial air recirculation. Some of the air dispersed by the impeller is returned to the impeller zone by the flow circulation induced and reduces the capacity to entrain fresh air into this zone. As frother reduces bubble size these smaller bubbles are more readily entrained in the water and the fraction of air recycled increases. This also reduces the density in the impeller zone and lowers power consumption (Figure 10).
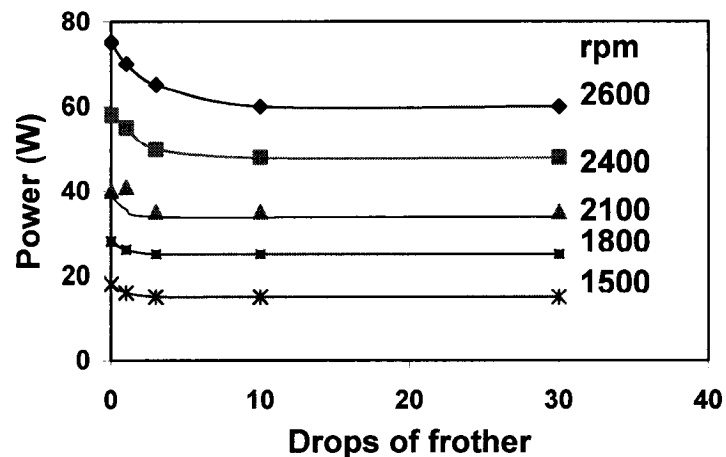
Figure 10. The power consumption as a function of frother addition and impeller speed: Wedag lab cell (redrawn from Arbiter et al., 1965)

2.3.2 Air-Liquid-Solid system

Compared with an air-liquid system, the presence of a solid phase acts to reduce aeration capacity, which diminishes as the solids concentration and particle size increase (Figure 11). These effects can be explained by segregation of solids toward the base of the tank and especially in the impeller region with consequent reduced capacity for air per unit volume of pulp. Figure 11 shows the power ratio as a function of the air flow rate with and without solids.
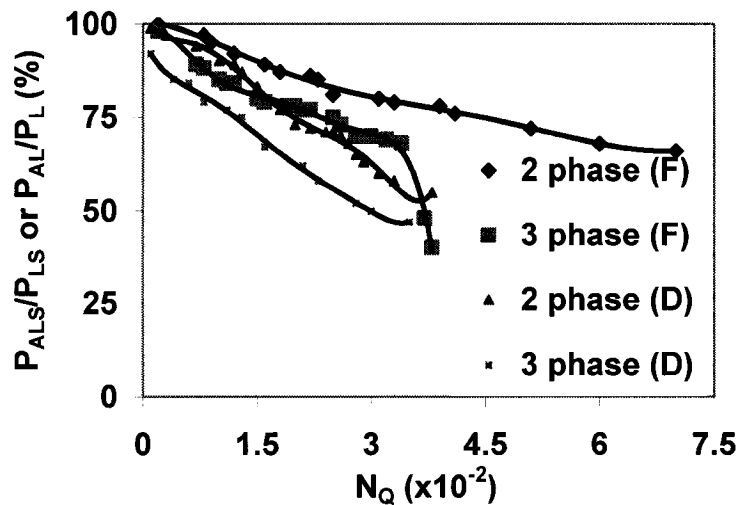
Figure 11. The power ratio as a function of air flow rate in the presence of solids: F-Fagergren lab cell, D-Denver lab cell (redrawn from Arbiter et al., 1969)

The introduction of air into a solid-liquid system reduces both the power consumption and the ability of the machine to suspend solids. These effects are more pronounced in the presence of a frother. All of these occurrences can be attributed to a lowering of the effective fluid density because of the presence of a solid, which is lowered still further when a frother is used due to its effect on decreasing bubble size and causing more gas to recycle (Arbiter et al., 1969).

With narrow size ranges of solids, flotation machines can display a sudden drop in the power ratio at a certain critical air flow number (see Fagergren cell, Figure 11), which coincides with sudden sedimentation of the particles. The sedimentation point occurs at higher values of N_Q as the particle size is decreased and as the concentration of solids in the system is decreased. The Denver lab cell did not display the effect of sudden sedimentation but gave a decreasing curve without an abrupt change of slope even with narrow size ranges. Observation indicates, however, that gradual sedimentation occurred as N_Q increased.

Chapter 3. Experimental part

3.1 Denver laboratory flotation cell

The cell consists of a PVC square shell with a volume of 5.2 L, measured by filling with water. The cell at the top was 22 cm x 16.8 cm. The diameter of impeller, suspended at the center, was 9.4 cm. The effective cross section was taken at the top of the cell minus the area of the impeller. The impeller at controlled speeds of rotation agitates the cell contents. The Denver unit has a variable speed mechanism allowing precise impeller speed adjustment. Test work was done at several impeller speeds as indicated on the supplied tachometer. Air enters via a hollow standpipe surrounding the impeller shaft. The action of the impeller draws air down the standpipe. The cell was operated in self-aspiration and forced air modes.
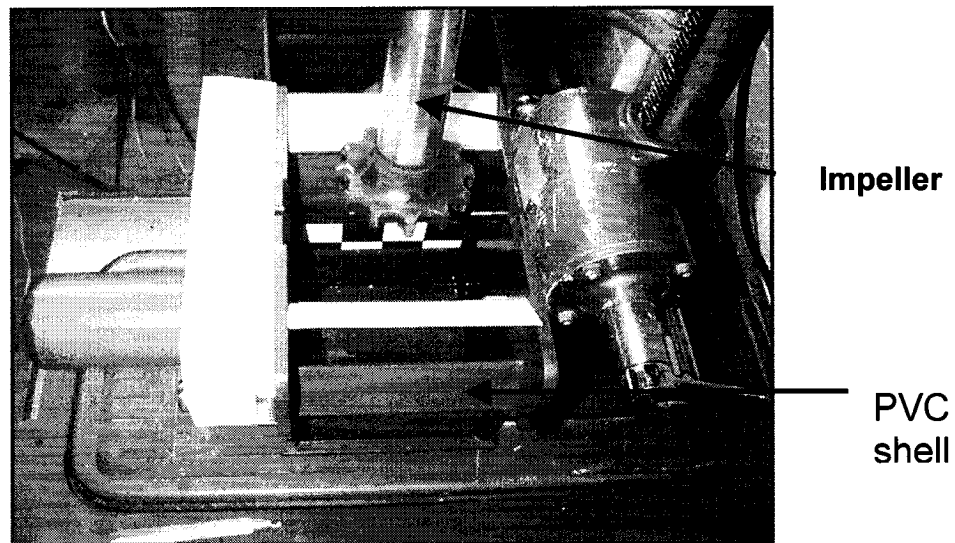
Figure 12. The Denver laboratory flotation cell

3.2 OPTO 22 and Fix MMI

The OPTO 22 is an industrial I/O interface manufactured by Transduction. It contains, in a single compact unit, analog boards, digital boards, and power

supply to drive the boards and external signals. All instruments were attached to the OPTO 22, which transmitted the signals to a computer. The analog and digital devices have 16 connecting points, each point may be connected in parallel with specific instruments through specific modules. The modules condition and convert the input and output signals, from analog to digital or from digital to analog. The modules have to be specified according to the I/O function, and to the range and kind of signal to be converted, i.e., 0-5 V, 4-20 mA and so on. The software used for data collection and control was a FIX MMI by Intellution.

In the experiments here, Opto 22 was used to control air flow rate using the Mass air flow meter and to obtain stable data using the McMillan. The McMillan air flow meter and the Mass air flow meter were connected to the Opto 22 and the computer registered the air flow rate. When forced air was used, the Opto 22 controlled the air flow rate.
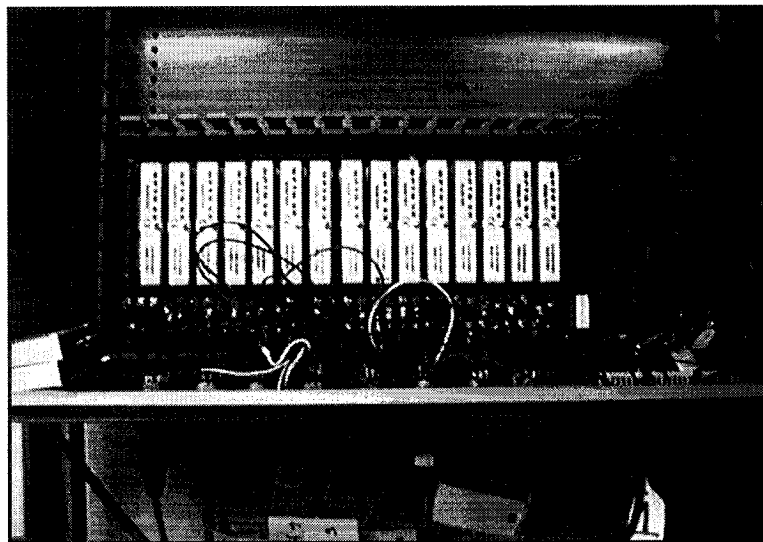
Figure 13. The OPTO 22

3.3 McMillan air flow meter

The McMillan air flow meter was chosen for use with aspirated air because it is a low pressure drop meter (maximum pressure drop~3 inch water). It features a 0-5VDC output and a range of 4-20 L/min.

33

The instrument uses an electro-optical system to sense flow rate. This system consists of an infrared diode beaming light through a glass window onto a turbine wheel. The spokes on the turbine wheel alternately reflect and absorb the light. The reflected light is sensed by a photo-diode, and electronics convert those pulses into a signal proportional to flow rate.

The working principle is based on measuring the pressure drop across a large orifice (to have a small pressure drop). As air passes, it is directed onto the teeth of the wheel using a precision-machined orifice. The flow impinges the wheel, spinning it faster as flow increases. This speed increase is directly proportional to the increase in flow rate. The flow meter adjusts the pressure difference using a special tube, thereby creating a low-pressure drop.
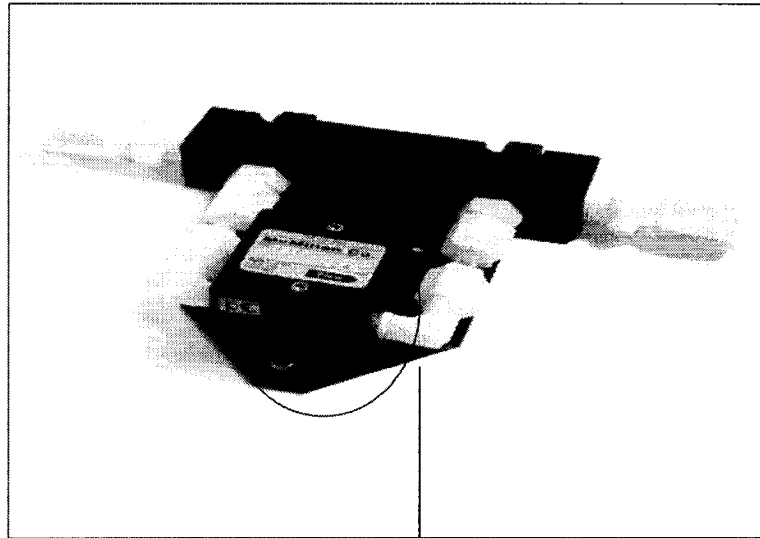
Figure 14. The McMillan air flow meter

advanced
electronics

infrared LED
and photodiode

glass
window
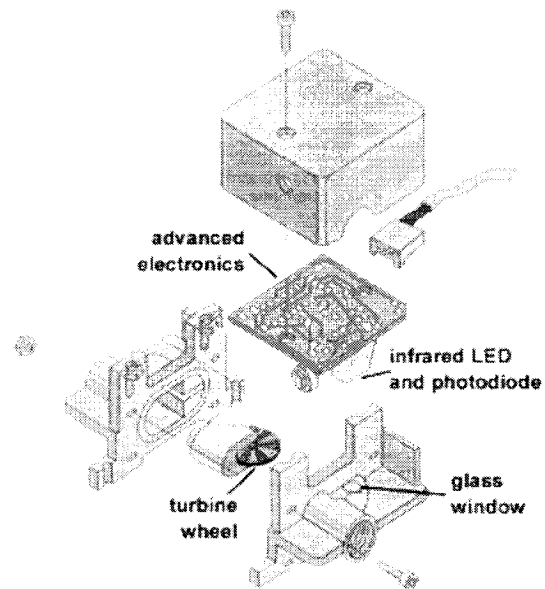
turbine
wheel

Figure 15. Breakdown of McMillan turbine wheel.

3.4 Bubble size analyzer

The device consists of a sealed glass viewing chamber (bubble viewer) and a sampling tube (Figure 16). The viewing chamber has a covered opening, allowing access to the chamber for cleaning. An object of a known diameter (3.05 mm) was installed on the viewing window to focus the camera, and to calibrate bubble size.

As bubbles rise into the chamber they encounter an inclined window (15 deg to vertical) and spread into a single layer as they slide up. A slope of 15 degrees gives a single layer of bubbles against the glass window thus giving the plane of focus and reducing the overlap of bubbles. This slope was determined by trial and error to give the desired single layer while minimizing potential bubble distortion at higher angles. The collection tube is immersed to the desired location below the froth. Bubble images were taken using a digital CCD camera, which is installed in front of the viewing chamber with diffused lighting from behind (the diffuser was simply layers of filter paper). Images were transferred to a computer and automatically processed using a commercial software package (Northern Eclipse v 6.0 from Empix Imaging).
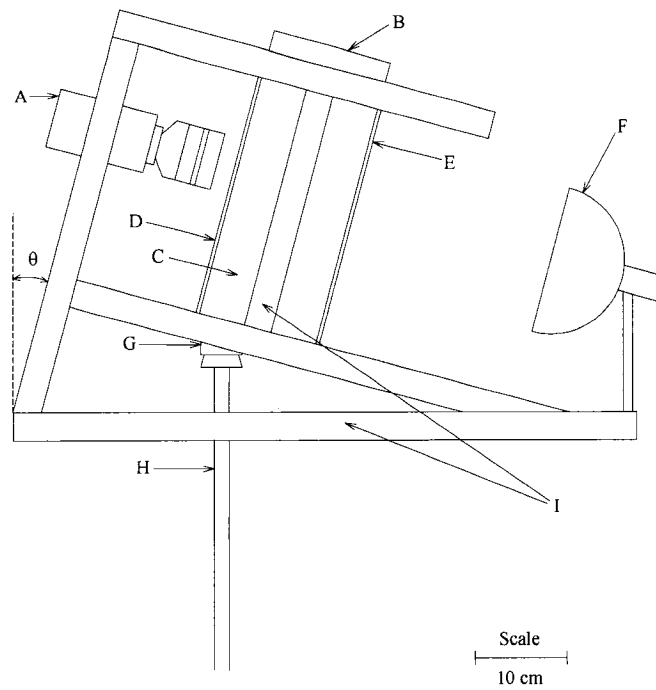
Figure 16. Scaled diagram of the McGill University bubble size measurement device. A: digital camera, B: filling cap, C: viewing chamber (bubble viewer), D: front window, E: back window, F: lamp, G: bubble viewer inlet, H: sampling tube, I: aluminum square bars (for support), θ: angle of the inclined window (15°).

3.5 Superficial gas velocity (J_g)

Superficial gas velocity is now quite commonly used to designate flowrate in a flotation machine. For a volumetric flowrate Q_g into a vessel of cross-sectional area A, J_g is given by:

$$J_g = \frac{Q_g}{A}$$

(3.1)

The Q_g is measured by the McMillan air flow meter when using aspirated air and by a mass flow meter when using forced air. Air flow rate measured by the mass

flow meter was referenced to 1 atm and 0°C. It was adjusted to the temperature and pressure conditions inside the flotation cell. The cell cross sectional area is $3.002 \times 10^{-2} \, m^2$.

3.6 Bubble size measurement

A bubble size is presented as a distribution and by a mean. Two means were used: the number mean diameter (d_{10}) and the Sauter mean diameter (d_{32}), calculated as follows:

$$d_{10} = \frac{\sum_{i=1}^{i=n} d_i}{N} \qquad (3.2)$$

$$d_{32} = \frac{\sum_{i=1}^{i=n} d_i^3}{\sum_{i=1}^{i=n} d_i^2} \qquad (3.3)$$

where

d_i = equivalent spherical bubble diameter.

n = sample size

N = number of bubbles

The d_{32} was principally used as it relates to the bubble surface area flux. (It gives the same value of S_b as calculated by summing over the bubble size distribution.)

3.7 Calibration of McMillan air flow meter

Before each set of tests, the McMillan air flow meter was calibrated. A typical result is shown in Figure 17. The relationship was linear and close to unity.

$$y = 0.9377x$$
$$R^2 = 1$$
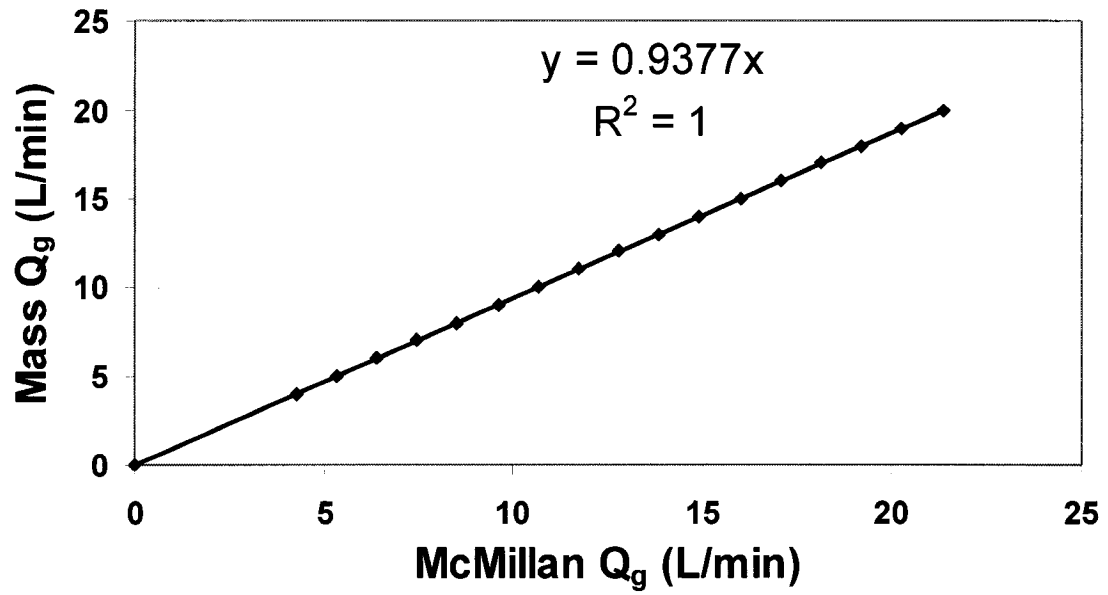
Figure 17. Calibration of McMillan air flow meter against mass flow meter

Chapter 4. Results and Discussion

4.1 Aspirated air

4.1.1 Superficial gas velocity

As shown in Chapter 2, when self-aspirating (or simply aspirating or entraining) air rate varies with impeller speed, frother concentration and solids content. These relationships were explored.

It was anticipated that there might be an effect of liquid level in the cell on air flow rate and bubble size. It proved difficult to control the level with a froth present. Hence, all experiments were made with no froth layer. The cell was always kept full of water or slurry by collecting and recycling any overflow. The experimental conditions are shown in Table 2.

Usually, laboratory flotation testwork is done at impeller speeds between 800 rpm and 1200 rpm. The flotation experiments in my research were done between 1400 to 2700 rpm, representing the minimum to register air flow with the McMillan model used and the maximum speed.

Table 2. Experimental conditions for superficial gas velocity measurement (frother: Dowfroth 250)

Impeller speed (rpm)	1400 - 2700
Frother concentration (ppm)	0, 5, 10, 30, 50
Solid concentration (w/w%)	0, 10, 20, 30

4.1.1.1 Reproducibility

A vital requirement of any experiment is reproducibility. Repeat tests were conducted at two conditions: 1600 rpm impeller speed and no frother (run 1); and

2500 rpm impeller speed and 50 ppm frother (run 2). Each was repeated five times. The results are given in Table 3.

Table 3. The results of reproducibility test on the air flow rate

	Run 1	Run 2
Test num	Q_g (L/m)	Q_g (L/m)
1	4.40	10.30
2	4.61	10.65
3	4.30	10.50
4	4.50	10.43
5	4.54	10.45
Sum	22.38	52.33
Average	4.48	10.47
Stan dev	0.12	0.13

The relative standard deviation (stand dev/mean) is 2.7% and 1.2% for run 1 and run 2, respectively, giving an average value, ca 2%. The standard deviation at any point was estimated by: value x 0.02 and is recorded on most figures.

4.1.1.2 Effect of frother concentration

Figure 18 shows the air flow rate as a function of impeller speed for five frother (Dowfroth 250) concentrations. Increasing speed increases the amount of aspirated air as expected. It also reveal that the use of higher impeller speeds than are commonly used in laboratory testwork will give more closely matching superficial gas velocity found in industrial plant practice (0.5-2.0 cm/s). The results demonstrate that operating a laboratory flotation cell at higher impeller speeds, results in data more closely related to industrial performance.

As frother is increased the air flow rate decreases at a given impeller speed, becoming approximately constant at high speed above ca. 30 ppm frother. The self-aerating capacity of a flotation machine decreases in the presence of frother. This result is explained by the effect of partial air recirculation (Arbiter et al., 1969). As the average retention time of the air bubbles increases with increasing

41

frother concentration because the bubble size decreases, this reduces the density in the impeller zone and thereby decreases the power to aspirate air.
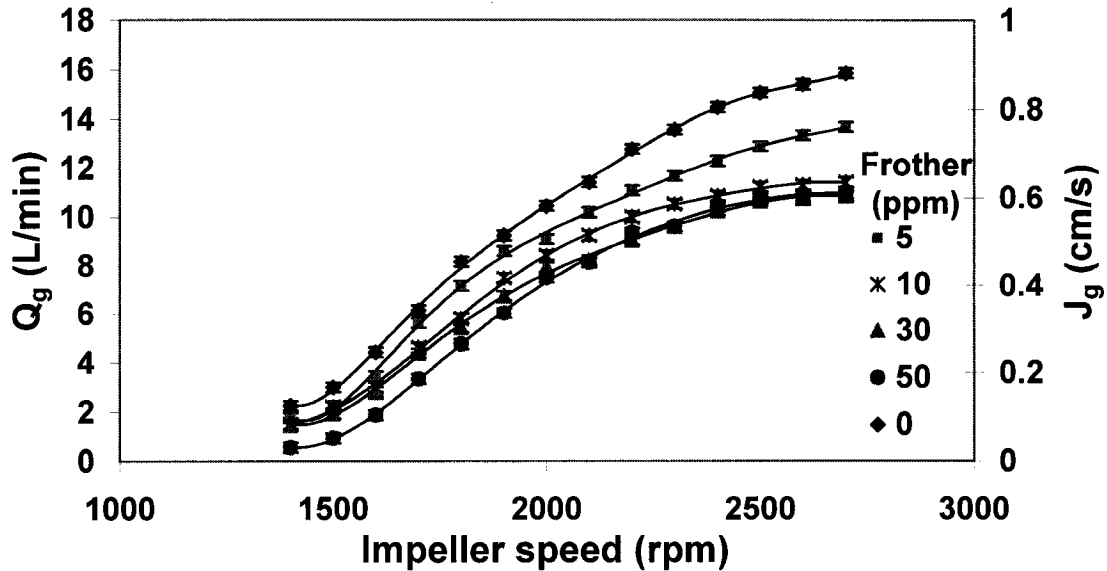
Figure 18. Air flow rate as a function of impeller speed for different frother concentrations

4.1.1.3 The effect of solids content

Figure 19 shows air flow rate as a function of impeller speed for a range of solids content using fine silica (-30μm). Between 0 and 10%w/w the air rate decreases but no further effect of increasing solids content occurs.

The self-aerating capacity of the flotation machine decreases in the presence of solids. This effect has been attributed to segregation of solids in the impeller region and a decrease of the density of pulp. The power consumption is directly proportional to the liquid or fluid density of the impeller zone. Therefore, the self aerating capacity decreases with solids (Arbiter et al., 1969).
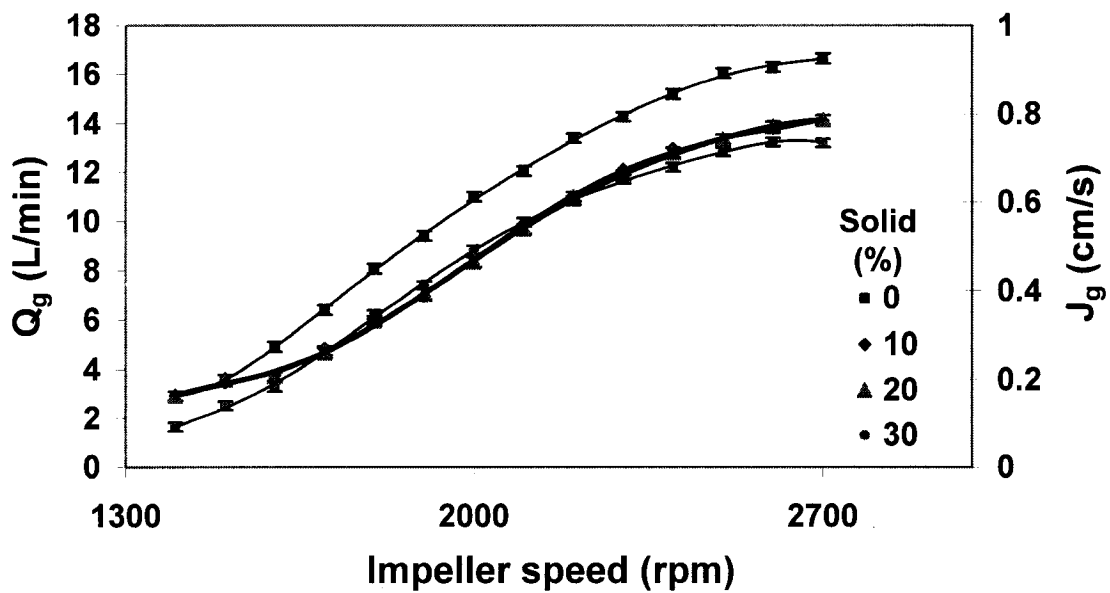
Figure 19. Air flow rate as a function of impeller speed at different solids content: frother concentration = 50 ppm)

4.1.2 Bubble size

4.1.2.1 Location

To begin, bubble size was measured at various locations in the cell. One purpose was to select the best sampling point for future measurements.

The measurements were performed twice at 25 locations (Figure 20). Each location is numbered. Sampling was done over an evenly spaced coordinate grid covering the cell cross section at several depths below the froth/pulp interface. This experiment was done at 100ppm frother (MIBC) concentration and 1400 rpm impeller speed.
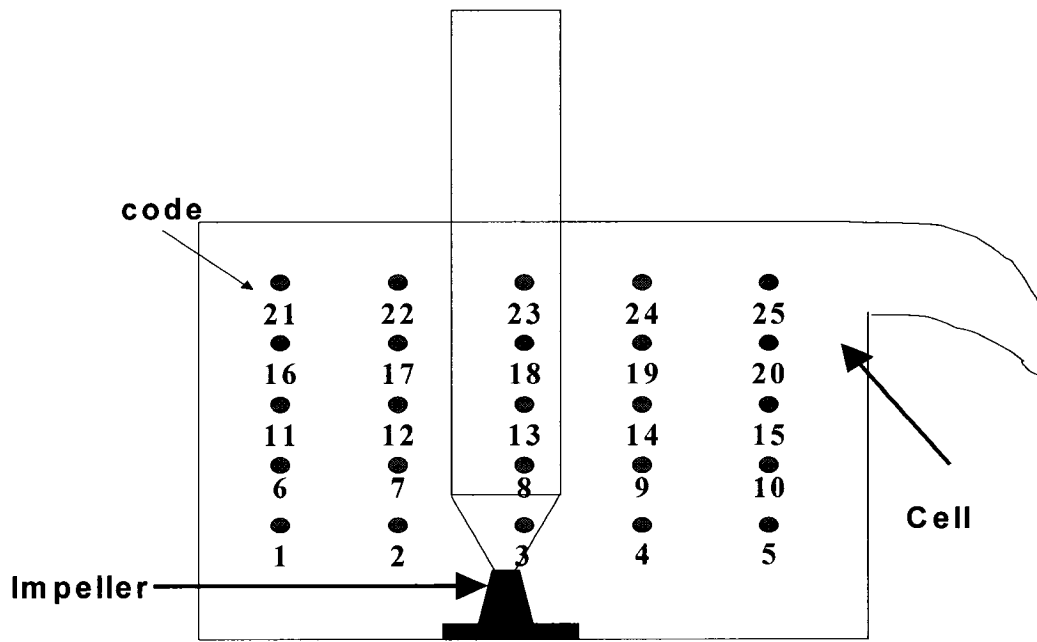
Figure 20. The location of bubble size measurement

The Sauter mean diameter (d_{32}) was plotted against the location (Figure 21). This reveals no obvious trend; the values for locations 1,2,3 may be considered high but locations 4,5 should be similar if being the lowest row mattered. And note, any other location coding system would have broken the apparent trend with locations 1 to 3. When comparing the two runs at the same location, there was little difference. Based on this test, it was decided to measure bubble size at point 24.
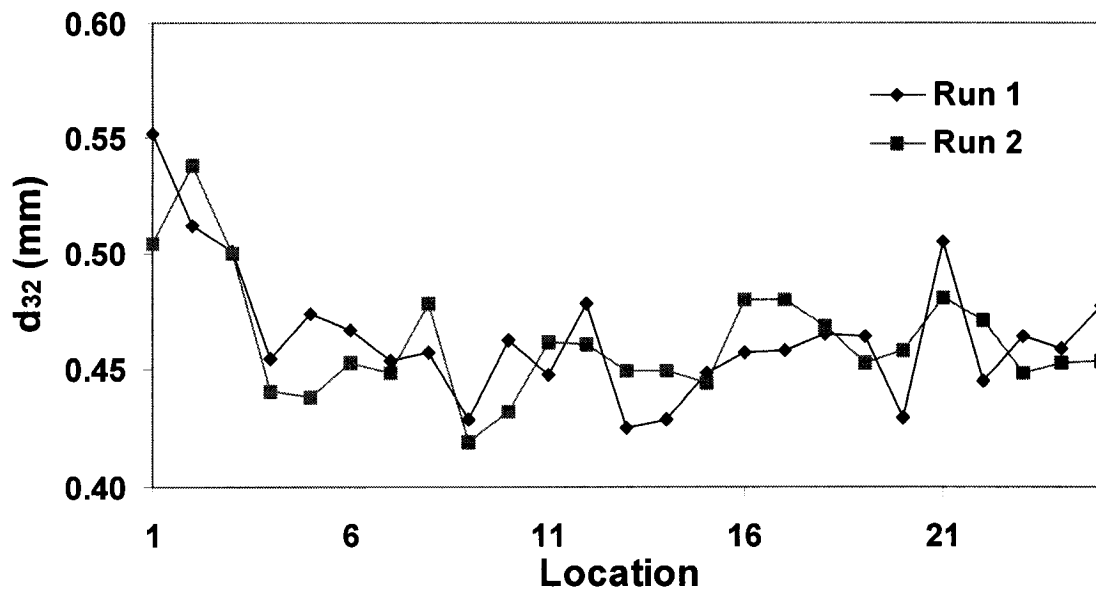
Figure 21. The results of location test.

4.1.2.2 Reproducibility

Repeat tests were conducted at two conditions: 1600 rpm impeller speed and 50 ppm of frother (run 1); and 2500 rpm impeller speed and 5 ppm of frother (run 2). Each was completely repeated five times. The results are given in Table 4.

Table 4. The results of reproducibility test of bubble size

Test num	Run 1		Run 2	
	d_{10} (mm)	d_{32} (mm)	d_{10} (mm)	d_{32} (mm)
1	0.30	0.36	0.65	0.95
2	0.36	0.47	0.62	0.91
3	0.26	0.33	0.69	1.00
4	0.24	0.32	0.59	0.87
5	0.23	0.31	0.57	0.87
Average	0.28	0.36	0.62	0.92
Stan dev	0.05	0.07	0.05	0.06

45

The relative standard deviation on d_{32} was 19% and 7% for runs 1 and 2, respectively, giving an average of ca. 13%. The standard deviation at any point was estimated by: value x 0.13 and is included on most figures.

4.1.2.3. Bubble size measurement in two phase

Bubble size measurement was performed first in air-water. The experimental conditions are presented in Table 5. Sixteen impeller speed-frother concentration combinations were tested.

Table 5. Experimental condition of bubble size measurement in two phase: Frother Dowfroth 250

Impeller speed (rpm)	1400, 1600, 1800, 2200, 2500, 2700
Frother concentration (ppm)	0, 5, 10, 50, 100

Examples of images are shown in Figure 22.
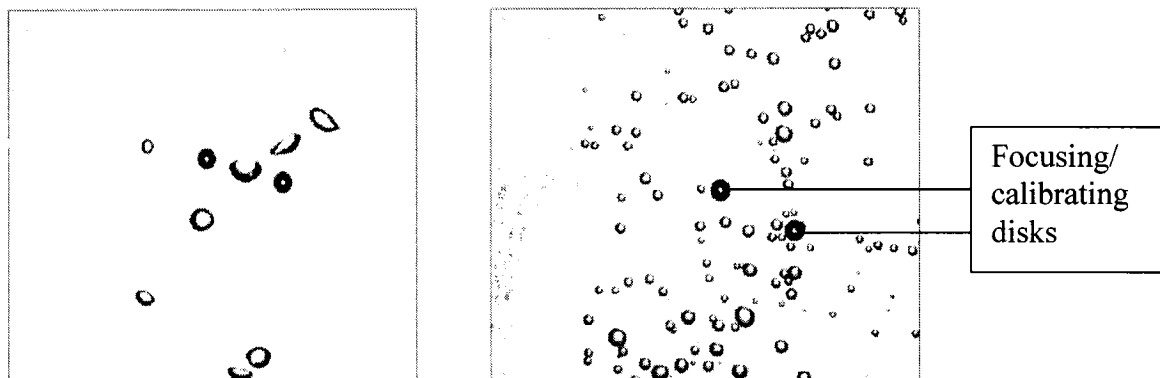
Figure 22. Example bubble images at a) 2500 rpm and 0 frother and b) 2500 rpm and 50 ppm frother: (Dowfroth 250)

It is clear that adding frother affected the bubble size markedly.

4.1.2.3.1 Effect of impeller speed

Figure 23 Indicates the influence of impeller speed on bubble size and includes the previous result for the effect on superficial gas velocity at two frother concentration.
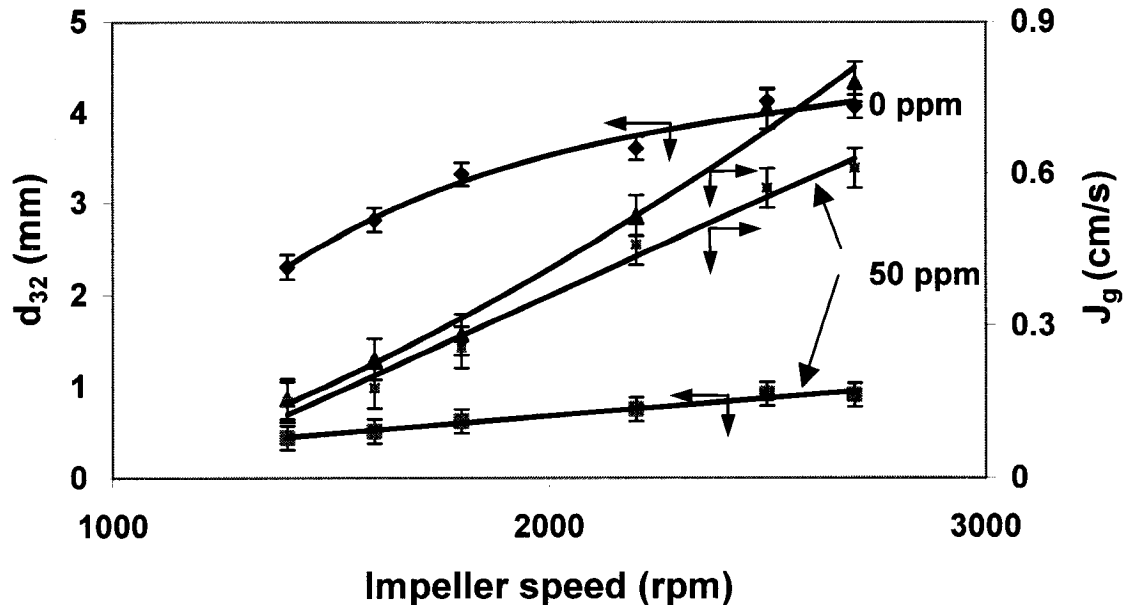
Figure 23. Bubble size and superficial gas velocity as a function of impeller speed

The results indicated that the bubble size increased with increasing impeller speed. This result was not expected until it is recalled that the gas rate, J_g, increases with impeller speed: the increase in d_b follows the increase in J_g, which is expected.

4.1.2.3.2 Effect of frother concentration

Figure 24 shows that the presence of frother reduced the mean bubble size. The bubble size decreased drastically at low frother concentrations then remained almost constant at high frother concentrations. The presence of frother is known to be the dominant factor in determining bubble size (Harris, 1976). Cho and Laslowski, (2002) introduced the concept of a critical coalescence concentration

above which frother does not further reduce bubble size. This appears to be close to 5ppm in the present condition.
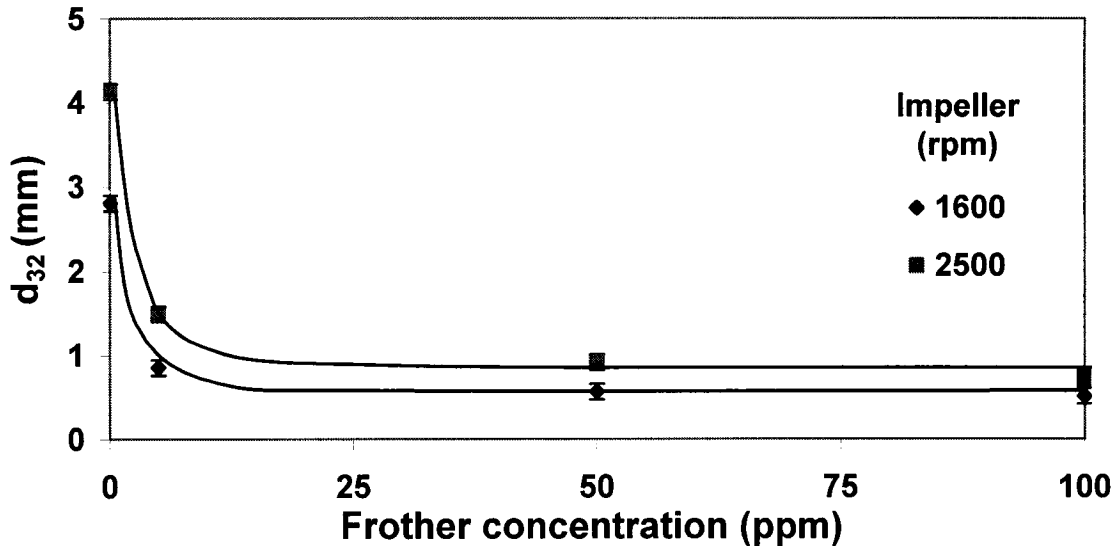
Figure 24. Bubble size as a function of frother concentration

Bubble size distributions are presented in Figures 25 and 26 on a cumulative volume basis. The distribution narrows and shifts to finer size on increasing frother concentration (Figure 25), again the dominant effect being at low dosage. The increase in size is evident as impeller speed increases (Figure 26).
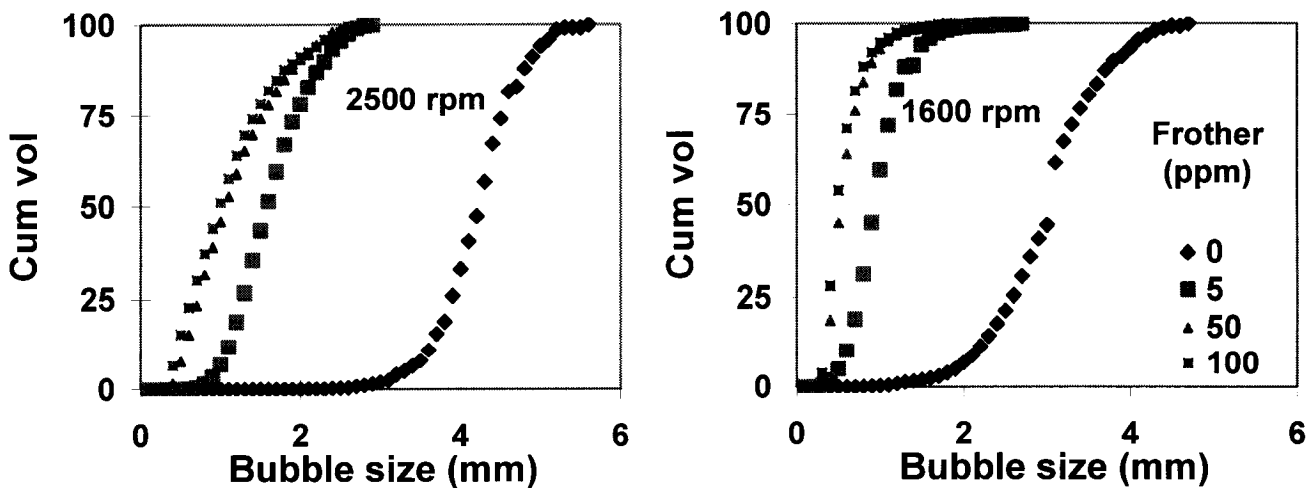
Figure 25. Bubble size distribution at different frother concentrations

It is evident that frother has much greater impact on bubble size distribution than impeller speed.
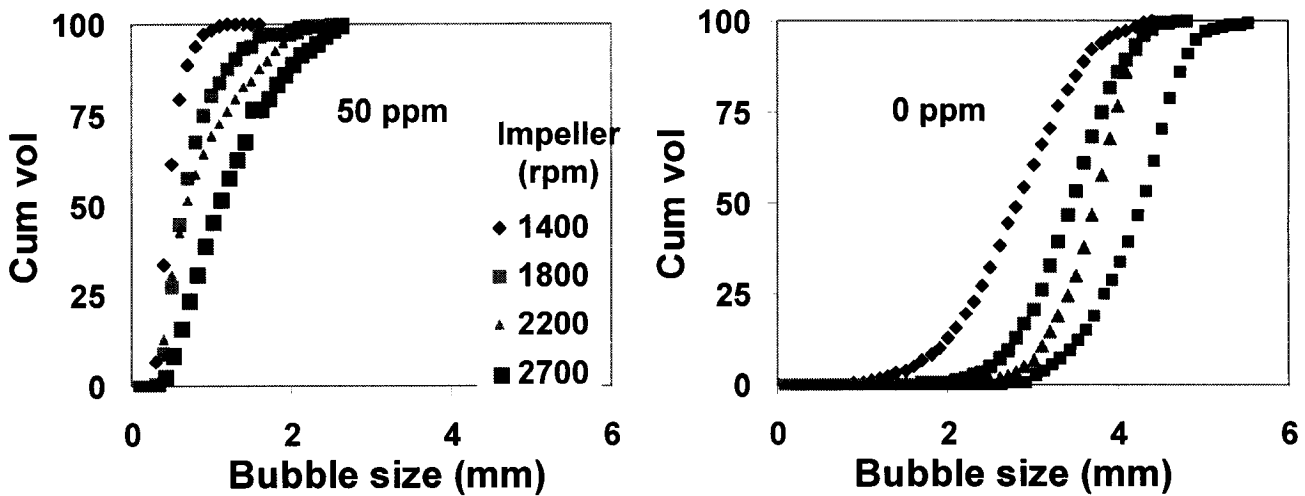
Figure 26. Bubble size distribution at different impeller speeds

4.1.2.3.3 Comparison between d_{10} and d_{32}

The d_{32} is always larger than the d_{10} and as the size distribution broadens this difference grows. The ratio d_{32}/d_{10}, therefore, carries information regarding the distribution width.

Figure 27 shows the ratios at 0 and 50 ppm as a function of impeller speed. As expected, d_{32} is always greater than d_{10}. With increasing speed, the ratio increases at 50 ppm, indicating the broadening of size distribution. The widening is biased to large bubbles, i.e., the population of large bubbles increases at the expense of the small ones.

However, this trend is not evident at 0 ppm. Interpretation is complicated by the fact that air rate changes with impeller speed which affects bubble size, i.e., there is an interaction between impeller speed and air rate on bubble size, which may affect the d_{32}/d_{10} ratio.
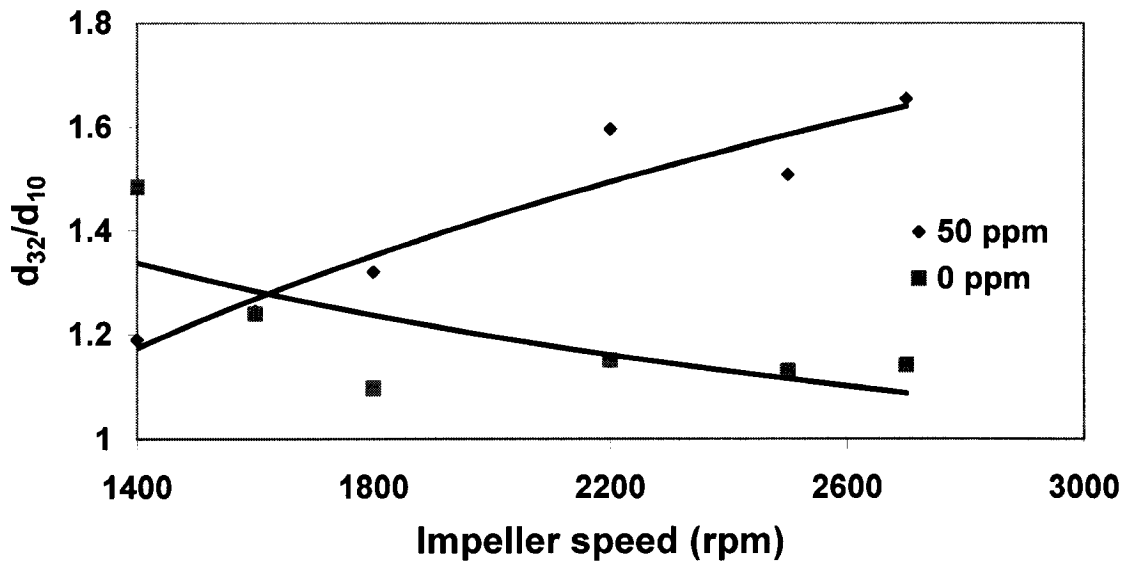
Figure 27. The ratio d_{32}/d_{10} as a function of impeller speed

Figure 28 shows that there is likely no relationship with frother concentration at 1600 rpm. However, the ratio increases at 50 ppm, indicating the broadening of size distribution at 2500 rpm.
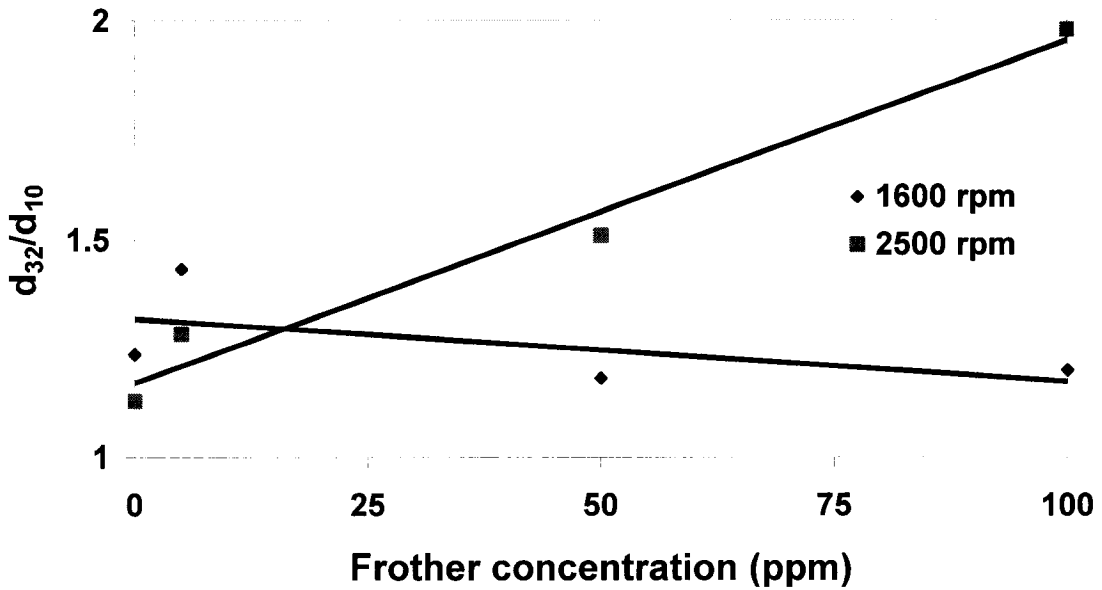
Figure 28. The ratio d_{32}/d_{10} as a function of frother concentration

4.1.2.4. Bubble size measurement in three phase

The solids were -30μm silica, which is hydrophilic under the conditions shown in Table 6. The purpose of these experiments was to determine the effect of solids content

Table 6. Experimental condition of bubble size measurement in three phase: Aspirated air, Frother Dowfroth 250

Impeller speed (rpm)	1600, 2500
Frother concentration (ppm)	50, 100
Solids content (w/w%)	10

O'Connor et al. (1990) and Tucker et al. (1994) claimed that the bubble size increased slightly in the presence of solids in tests on a flotation column. Ityokumbul et al. (1995) claimed that the effect of solids is negligible except at low gas velocities for which complete suspension of solids from the gas distributor was not observed. Banisi et al. (1994) inferred from gas holdup measurements that solids had no effect on bubble size. They did note that solids (at least hydrophobic ones) may adsorb frother and this in turn may promote coalescence, i.e., an indirect effect on bubble size.

Experiments were designed to test the effect of solids on the bubble size and to check for possible frother adsorption. Bubble size was first measured in two phase, then after solids addition. After this, the suspension was filtered to remove the solids and the bubble size measured again. The results are given in Figures 29 and 30.
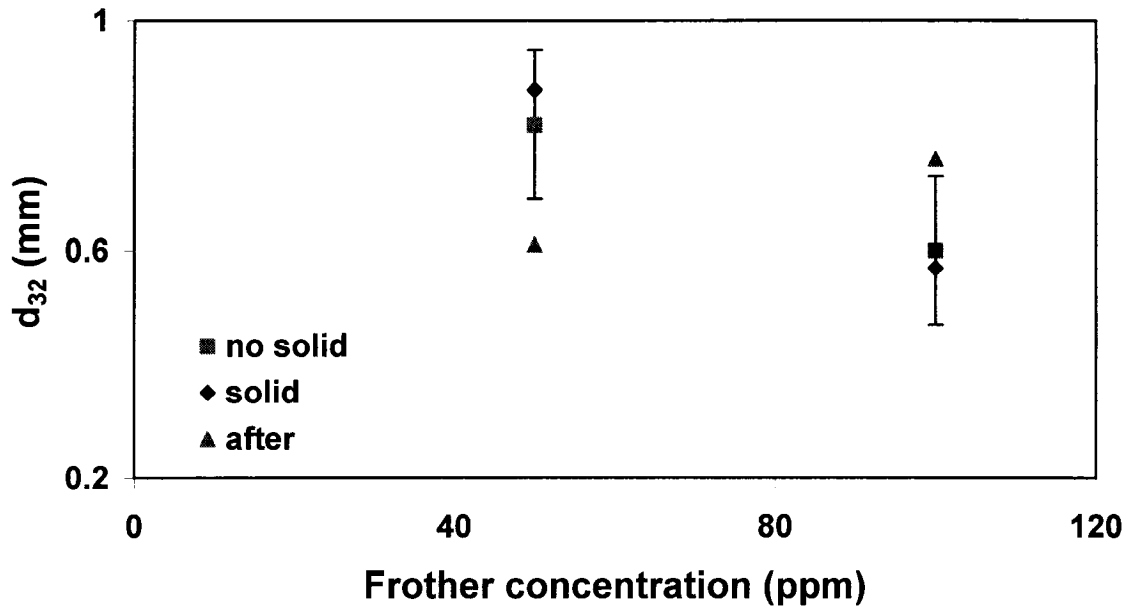
Figure 29. Effect of solids on bubble size: Impeller speed 2500 rpm (Standard deviation is included for three phase only for clarity).
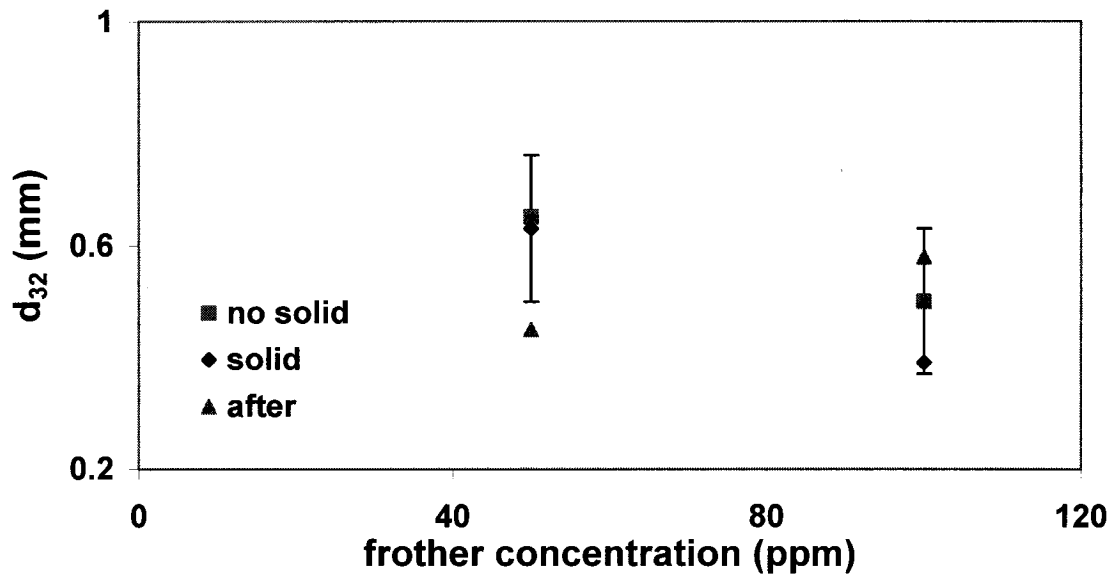
Figure 30. effect of solids on bubble size: impeller speed 1600 rpm (Standard deviation is included for three phase only for clarity).

The results reveal no trend attributable to presence of solids. In three of the four tests the no solids/solids bubble size are virtually unchanged and all are within experimental repeatability. Interestingly, the largest change is after solids removal but this is random, twice the bubble size decreasing, twice increasing. The conclusion is that fine hydrophilic silica does not affect the bubble size, either directly or indirectly by adsorbing frother. There was an experimental issue that the solids content was slowly diluted during the experiment. The slurry was recycled to maintain level, but this could not guarantee that all the solids were recycled. It is recommended to improve the experimental method and recycle the suspension using a pump.

4.1.3. Bubble surface area flux

One objective was to use bubble surface area flux to characterize the cell gas dispersion. The S_b is calculated from J_g and d_{32}. Figure 31 shows an approximately linear relationship with impeller speed. The dominant contribution to S_b is the increase in J_g with impeller speed, which more than offsets the increase in d_{32} (see Figure 23).
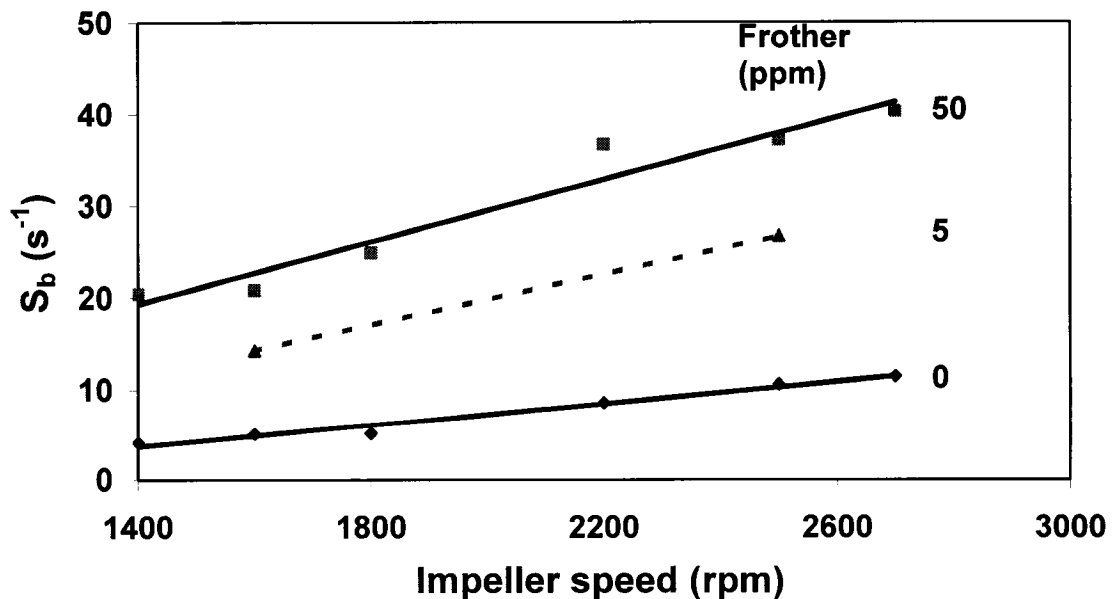
Figure 31. Bubble surface area flux as a function of impeller speed

Figure 32 shows S_b as a function of frother concentration. In this case, the decrease in bubble size more than offsets the decrease in J_g as frother dosage is increased (see Figure 25).
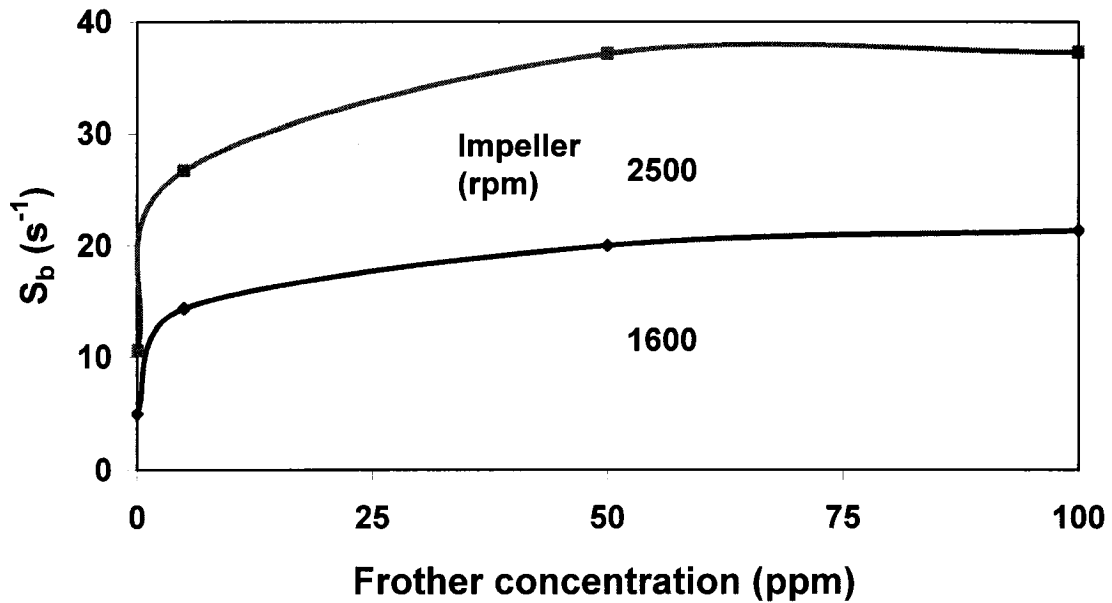
Figure 32. Bubble surface area flux as a function of frother concentration

Figure 33 shows S_b versus superficial gas velocity controlled by changing impeller speed; i.e., it is an another way to present Figure 33.
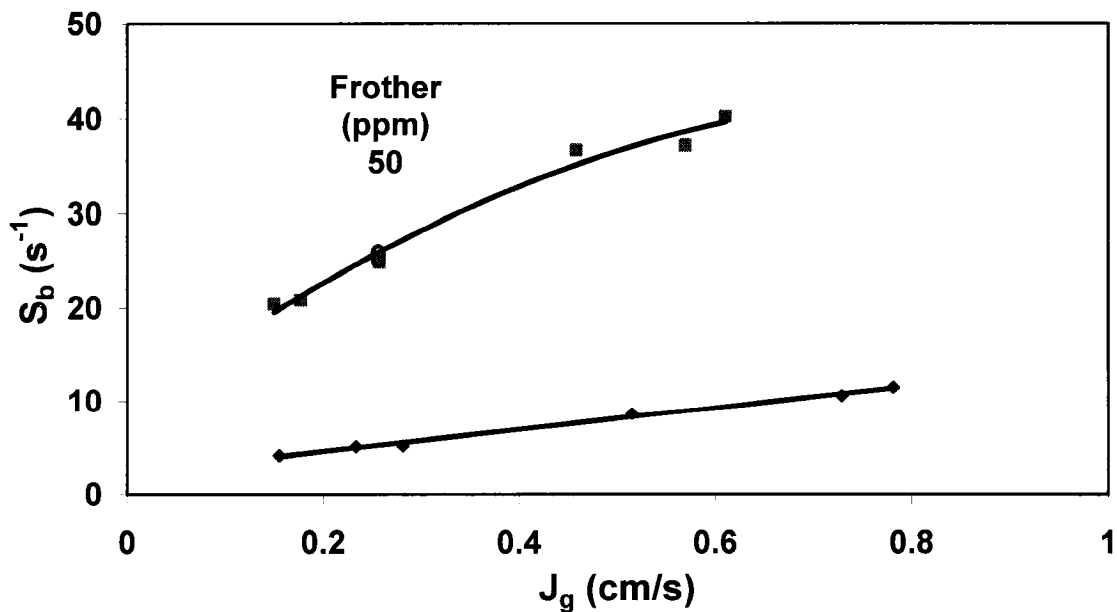
Figure 33. S_b as a function of J_g

4.2 Forced air

4.2.1 Bubble size measurement

Bubble size measurement was performed in two phase using forced air. The experimental conditions are presented in Table 7. The mass air flow meter was used, calibrated and connected to the Opto 22, which also controlled the air rate. Ten impeller speed-frother concentration combinations were tested.

Table 7. Experimental conditions for bubble size measurement in two phase using forced air (frother, Dow froth 250)

Impeller speed (rpm)	1600, 2500
Frother concentration	50
Air flow rate (L/m)	2.5, 5, 10, 15, 20
Air flow rate (cm/s)	0.14, 0.28, 0.56, 0.83, 1.11

4.2.1.1 Effect of impeller speed and air flow rate

Figure 34 shows bubble size increases with J_g and decreases with increasing impeller speed in contrast to the aspirated air condition. The impeller effect now corresponds to expectation.

It is recommended that in order to have similar experimental conditions as in industry that the forced air option is used in the laboratory Denver cell. Certainly to investigate the effect of impeller speed on the bubble size or metallurgical performance it is much better to use forced air rather than using aspirated air.
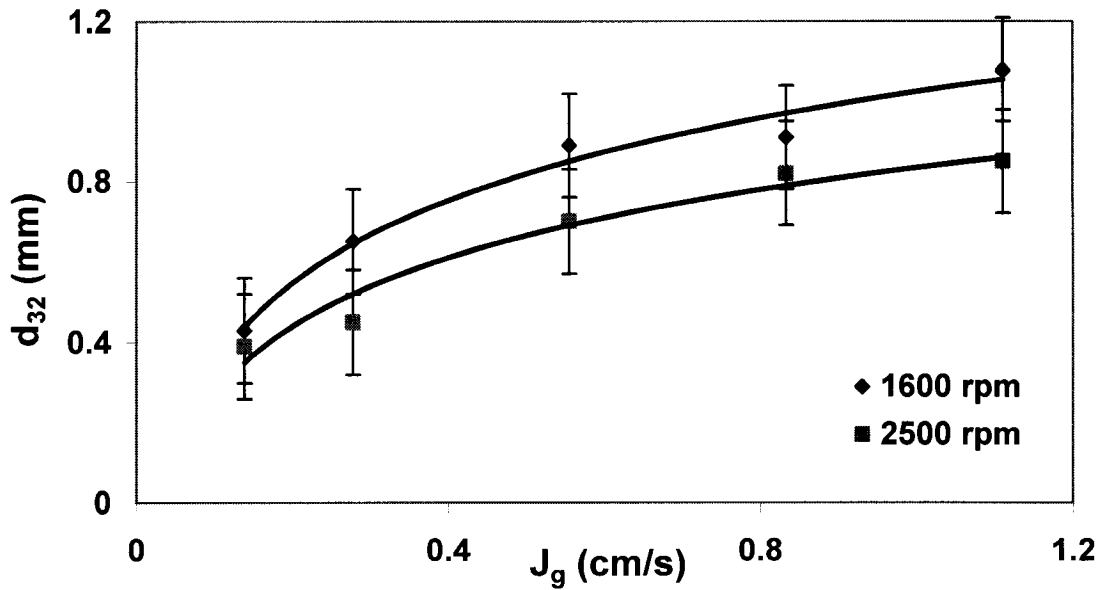
Figure 34. The Sauter mean bubble size as a function of J_g: frother 50 ppm

4.2.1.2 Comparison between d_{10} and d_{32}

With increasing J_g, the ratio increases at both impeller speeds, showing broadening of the distribution (Figure 35). At a given J_g, increasing impeller speed reduces the ration, i.e., narrows the distribution.
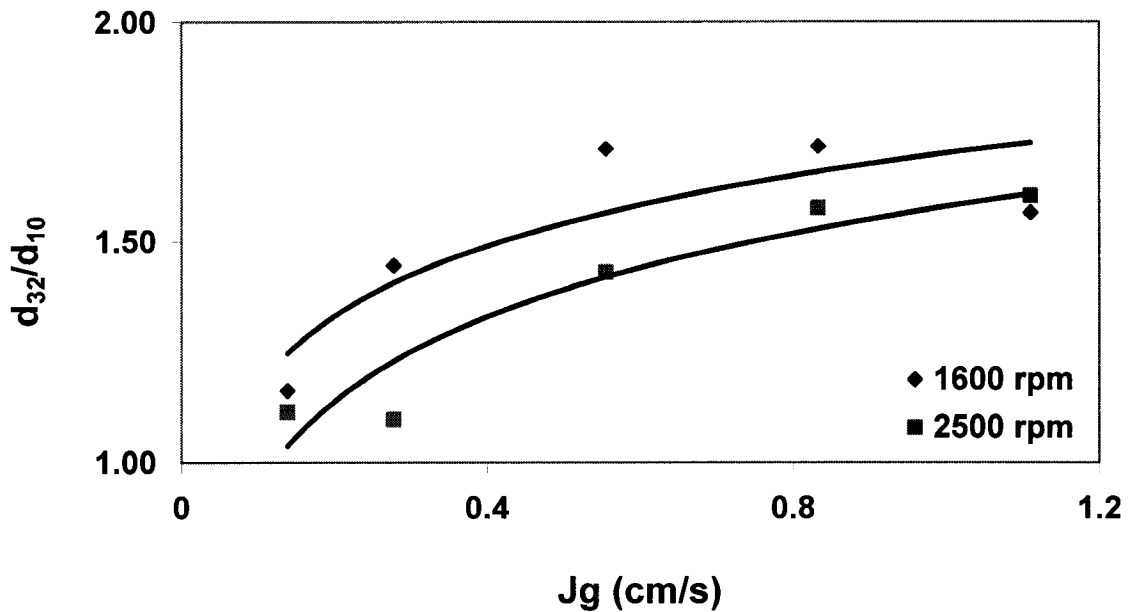
Figure 35. d_{32}/d_{10} as a function of J_g

4.2.3 Bubble surface area flux

Figure 36 shows that S_b increased with increased J_g and impeller speed. The range of S_b is now up to $80s^{-1}$, nearly twice that using aspirated air, which is included for reference. Vera et al. (1999) noted most laboratory flotation cells produce low S_b values ($< 30s^{-1}$) and generate bubble sizes greater than 1.2 mm. In response, they designed a new, so-called high S_b cell. Here it is shown that S_b values up to $80s^{-1}$ are reached in a standard cell provided forced air is used. Considerably smaller bubbles than suggested by Vera et al. (1999) (the smallest d_{32} was 0.39 mm) were produced in this work using the Denver laboratory flotation cell with forced air. Finch et al. (2000), re-working mechanical laboratory cell data of Szatkowski et al. (1987), showed S_b values up to $120s^{-1}$.
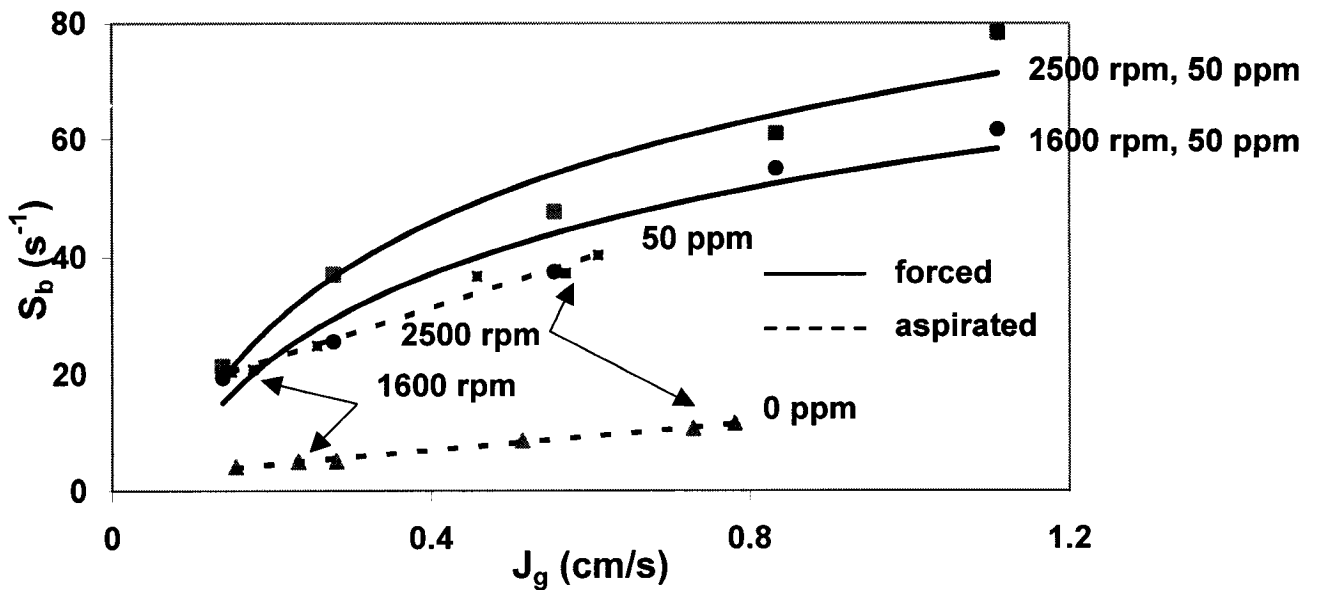
Figure 36. S_b versus J_g using forced air and aspirated air

Chapter 5. Conclusions

Aspirated air

J_g measurement

- The average relative standard deviation for J_g measurement was ca. 2%.

- The amount of entrained air increased with increasing impeller speed due to the suction generated by the impeller: suction α (impeller speed)^2.

- The amount of entrained air decreased with increasing frother concentration at a given impeller speed, becoming approximately constant at high impeller speed. This can be attributed to partial air recirculation. The increase of the average gas retention time with increasing frother concentration reduces the density in the impeller zone and thereby decreases the power to aspirate air.

- The amount of entrained air decreased with increasing solids content. This effect has been attributed to the decrease of fluid density in the zone surrounding the impeller by segregation of solid. This results in a decrease of power consumption and air flow rate.

- For a self-aerating flotation machine, air flow rate is not an independent variable but varies with impeller speed, frother concentration and solids content.

- Among operating variables, impeller speed has been shown to have the most effect on entrained air flow rate.

- The use of impeller speeds higher than commonly used in laboratory testwork will give superficial gas velocities closer to those found in industrial practice.

Bubble size measurement

- There was no significant effect of location on bubble size measurement.

- The relative standard deviation on d_{32} was ca. 13%.

- The bubble size increased with increasing impeller speed, attributed to the increase in J_g.

- The presence of frother reduced the bubble size. The decrease was most notable at low frother concentrations then remained almost constant at high frother concentrations. The critical coalescence concentration appeared to be close to 5 ppm for the present condition.

- Solids did not affect the bubble size

- Frother was the dominant factor in determining bubble size.

- There was no consistent trend in the ratio d32/d10 (used to infer width of size distribution) with frother of impeller speed.

Bubble surface area flux

- There was a linear relationship between S_b and impeller speed. The dominant contribution to S_b was the increase in J_g with impeller speed, which more than offset the increase in d_{32}.

- The S_b increased with increasing frother concentration. The decrease in d_{32} with increasing frother concentration more than offset the decrease in J_g as frother dosage is increased. The range of S_b was up to $40s^{-1}$.

Forced air

Bubble size measurement

- The d_{32} decreased with increasing impeller speed and decreasing J_g. The impeller effect now corresponded to expectation.

- With increasing J_g, the d_{32}/d_{10} increased with set impeller speed, showing broadening of the size distribution.

- To have similar experimental conditions as in industry, the forced air option is recommended.

Bubble surface area flux

- The S_b increased with increasing impeller speed and J_g. The range of S_b was up to $80s^{-1}$ nearly twice that using aspirated air. S_b using forced air was larger than that using aspirated air. Smaller bubbles, down to $d_{32}=$ 0.39 mm were produced using forced air, considerably smaller than suggested by Vera et al. (1999) in a Denver laboratory flotation cell.

Chapter 6. References

Ahmed. N., Jameson. G.J., 1985. The effect of bubble size on the rate of flotation of fine particles. IJMP, 14, 195-214.

Arbiter, N., Harris, C.C., Steininger, J., 1964. Power requirement in multi-phase mixing.AIME Transactions, Vol. 229, pp 70-78.

Arbiter, N., Harris, C.C., Yap, R., 1968. A hydrodynamic approach to flotation scale-up. VIII International Mineral Processing Congress, Leningrad, Paper D19.

Arbiter, N., Harris, C.C., Yap, R., 1969. Flotation cell hydrodynamics. Trans. Am. Inst. Min. Eng, 244, 134-148.

Arbiter, N., Steininger, J., 1965. Hydrodynamics of flotation machines. Mineral processing, Pergamon press, New York, pp. 70-78.

Banisi, J.A., Finch, J. A., Laplante, A.R., Weber, M.E., 1994. Effect of solid particles on gas holdup in flotation columns-inverstigation of mechanisms of gas holdup reduction in presence of solids. Chemical Engineering Science, Vol. 50, pp. 2239-2334.

Brewis, T., 1991. Flotation cells. Mining Mag, June, 383-393.

Brewis, T., 1996. Flotation cells. Mining Mag, July, 18-24.

Chen, F., Gomez, C.O., Finch, Z.A., 2001. Technical note: bubble size measurement in flotation machines. Minerals Engineering, 14(4), pp. 427-432.

Cho, Y.S., Laskowski, J.S., 2002. Effect of flotation frothers on bubble size and foam stability. Int. J. Miner. Process, 64, 69-80.

Deglon, D.A., Egya-mensah, D., Franzidis, J.P., 2000. Review of hydrodynamics and gas dispersion in flotation cells on South Africa plantinum concentrators. Minerals Engineering, Vol. 13, No. 13, pp. 235-244.

Dobby, G.S., Finch, J.A., 1990. Column Flotation. Pergamon Press, New York.

Finch, J.A., Gomez, C.O., Hardie, C., Leichtle, G., 1999. Processings-31st Annual Meeting of the Canadian Mineral Processors, pp. 199-210.

Finch, J.A., Xiao, J., Hardie, C., Gomez, C.O., 2000. Gas dispersion properties: Bubble surface area flux and gas holdup. Minerals Engineering, Vol. 13, pp. 365-372.

Gorain, B.K., 1996. pH D Thesis, University of Queensland.

Gorain, B.K., Franzidis, J. P., Manlapig, E. V., 1997. Effect of bubble surface area flux on flotation performance. Minerals Engineering, Vol.10, pp. 367-379.

Gorain, B.K., Franzidis, J. P., Manlapig, E. V., 1999. The empirical prediction of bubble surface area flux in mechanical flotation cells from cell design and operating data. Minerals Engineering, Vol.12, pp. 309-322.

Harris, C.C., 1976. Flotation machines, in Flotation A.M. Gaudin Memorial Volume, Vol. 2. (Ed. M. C. Fuerstenau), AIME, pp. 753-815.

Harris, C.C., N. Aribiter., M.J. Musa., 1983. Mixing and gangue dispersion in flotation machine pulps. Int, J. Miner. Proc., 10, pp. 45-60.

Harris, C.C., N. Aribiter., M.J. Musa., 1983. Mixing and gangue dispersion in flotation machine pulps. Int, J. Miner. Proc., 10, pp. 45-60.

Harris, C. C., S, Khandrika, S. M., 1984a. Impeller/stator interactions in a laboratory flotation machine-the effect of wear on suction. International Journal of Mineral Processing, 12, 251-261.

Harris, C, C., Khandrika, S. M., 1984b. Oscillations in a laboratory flotation machine. International Journal of Mineral Processing, 12, 263-271.

Harris, C.C., Khandrika, S. M., 1985a. Short communication, Power technology, 45, pp. 95-97

Harris, C.C., Khandrika, S. M., 1985b. Flotation machine design: Important hydrodynamic effects; Slight geoketrical causes. Power technology, 43, pp. 243-248

Harris, C.C., Khandrika, S. M., 1985c. Flotation machine design: Impeller-stator interaction. Power technology, 43, pp. 273-278

Hernandez-Aquilar, J.R., Gomez, C.O., Finch, J.A., 2002. A technique for the direct measurement of bubble size distributions in industrial flotation cells. 34th annual meeting of the CMP.

Ityokumbul,.M. T., Kosaric, N., Bulani, W., 1995. Effect of fine solids and frother on gas hold-up and liquid mixing in a flotation column. Minerals Engineering, Vol. 8, pp. 1369-1380.

Jameson, G.J., Nam, S., Moo Yoong, M., 1977. Physical factors affecting recovery rates in flotation. Miner. Sci. Eng, 9(3), 103.

Klimpel, R.R., Dhansen, R., Fee, B.S., 1986. Selection of flotation reagents for mineral flotation. In design and Installation of concentration and dewatering circuit, Ed: Mular, A.L., Anderson, M.A., Chapter 26, pp. 384-404.

Laplante, A.R., Toguri, J.M., 1983a. The effect of air flow rate on the kinetics of flotation. Int. Jour. Min. Proc. 11, 203-219.

O'Conner, C.T., Randall, E.W., Goodall, C.M., 1990. Measurement of the effects of physical and chemical variables on bubble size. International Journal of Mineral Processing, 28(1-2), 139-149.

Oyama, Y., Endoh, K., 1955. Power characteristics of gas-liquid contacting mixers. Chem. Eng, Tokyo, 19, 2.

Szatkowski, M., 1987. Minerals and Metallurgical Processing, 4(1), 37-40.

Tucker, J.P., Delgon, D.A., Franzidis, J.P., Harris, M.C., O'Conner, C.T., 1994. Evaluation of a direct method of bubble size distribution measurement in a laboratory batch flotation cell. Minerals Engineering, 7(5-6), 667-680.

Vera, M.A., Franzidis, J-P., Manlapig, E.V., 1999. The JKMRC high bubble surface area flux flotation cell. Minerals Engineering, 12(5), 477–484.

Wills, B.A., 1992. Mineral processing technology. Pergamon Press. New York. Young, P., 1982. Flotation machines. Min. Mag, 146, 35.

Chapter 7. Appendices

Table 7-1: Summary of calibration of McMillan air flow meter with mass flowmeter

Table 7-2: Summary of measurement of air flow rate with different frother concentration

Table 7-3: Summary of measurement of air flow rate with different solids content

Table 7-4: Summary of location test

Table 7-5: Summary of bubble size measurement in two phase using self aspirated air

Table 7-6: Summary of bubble size measurement in three phase using self aspirated air

Table 7-7: Summary of bubble size measurement in two phase using forced air

Table 7-1. Summary of calibration of McMillan air flow meter with mass flowmeter

Air flow rate (Mass) (L/min)	Temperature (°C)	Air flow rate (McMillan) (L/min)
4	18.3	4.3
5	18.3	5.3
6	18.3	6.4
7	18.3	7.5
8	18.3	8.5
9	18.3	9.6
10	18.3	10.7
11	18.3	11.7
12	18.3	12.8
13	18.3	13.9
14	18.3	14.9
15	18.3	15.9
16	18.3	17.1
17	18.3	18.1
18	18.3	19.2
19	18.3	20.3
20	18.3	21.3

Table 7-2. The summary of measurement of air flow rate with different frother concentration

Impeller speed (RPM)	Air flow rate (L/min)			
	Frother concentration (ppm)			
	0	5	50	100
1400	2.25	1.76	1.46	1.50
1500	3.00	2.25	1.95	2.21
1600	4.43	3.45	2.81	3.00
1700	6.15	5.63	4.39	4.61
1800	8.18	7.16	5.44	5.81
1900	9.26	8.63	6.75	7.50
2000	10.46	9.11	7.95	8.44
2100	11.43	10.02	8.25	9.26
2200	12.79	11.10	9.08	10.01
2300	13.58	11.70	9.64	10.54
2400	14.48	12.30	10.28	10.88
2500	15.08	12.90	10.65	11.25
2600	15.42	13.35	10.76	11.33
2700	15.87	13.69	10.88	11.44

Table 7-3. Summary of measurement of air flow rate with different solid contents

Impeller speed (RPM)	Air flow rate (L/min)			
	Solids content (%)			
	0	10	20	30
1400	2.74	2.74	2.74	1.53
1500	3.38	3.26	3.38	2.36
1600	4.61	3.53	3.49	3.08
1700	6.00	4.54	4.39	4.46
1800	7.58	5.59	5.59	5.81
1900	8.81	6.53	6.60	6.94
2000	10.31	8.03	7.84	8.29
2100	11.29	9.26	9.08	9.33
2200	12.57	10.35	10.31	10.16
2300	13.39	11.36	11.14	10.99
2400	14.25	12.25	12.00	11.44
2500	15.04	12.42	12.53	12.04
2600	15.26	12.94	13.02	12.42
2700	15.60	13.24	13.28	12.38

Table 7-4: Summary of location tests

Location	Run 1		Run 2	
	d_{32} (mm)	d_{10} (mm)	d_{32} (mm)	d_{32} (mm)
11	0.552	0.396	0.504	0.390
12	0.512	0.384	0.538	0.396
13	0.501	0.371	0.500	0.374
14	0.455	0.324	0.441	0.355
15	0.474	0.344	0.438	0.354
21	0.467	0.341	0.453	0.336
22	0.454	0.350	0.449	0.339
23	0.457	0.347	0.478	0.326
24	0.429	0.332	0.419	0.322
25	0.463	0.328	0.432	0.308
31	0.448	0.326	0.462	0.348
32	0.478	0.361	0.461	0.344
33	0.425	0.310	0.450	0.329
34	0.429	0.317	0.450	0.329
35	0.449	0.342	0.444	0.305
41	0.457	0.340	0.480	0.365
42	0.458	0.336	0.480	0.353
43	0.465	0.340	0.469	0.342
44	0.464	0.341	0.453	0.343
45	0.430	0.326	0.458	0.344
51	0.505	0.366	0.481	0.388
52	0.445	0.353	0.371	0.380
53	0.464	0.335	0.449	0.344
54	0.459	0.342	0.453	0.336
55	0.477	0.357	0.454	0.327
Average	0.465	0.344	0.463	0.347

Table 7-5: Summary of bubble size measurement in two phase using aspirated air (cross section area of a lab cell=3.002x10^{-2} m^2)

Impeller (rpm)	Frother (ppm)	Q_g (L/min)	J_g (cm/s)	d_{10} (mm)	d_{32} (mm)	d32/d10	S_b (s^{-1})
1400	0	2.8	0.16	1.55	2.30	1.48	4.06
1600	0	4.2	0.23	2.27	2.81	1.24	4.99
1800	0	5.1	0.28	3.03	3.32	1.10	5.09
2200	0	9.3	0.52	3.14	3.61	1.15	8.56
2500	0	13.1	0.73	3.66	4.13	1.13	10.59
2700	0	14.1	0.78	3.57	4.07	1.14	11.51
1400	50	2.7	0.15	0.37	0.44	1.19	20.45
1600	50	3.2	0.18	0.41	0.51	1.24	20.82
1800	50	4.6	0.26	0.47	0.62	1.32	24.89
2200	50	8.3	0.46	0.47	0.75	1.60	36.65
2500	50	10.3	0.57	0.61	0.92	1.51	37.14
2700	50	11.0	0.61	0.55	0.91	1.65	40.23
1600	5	3.7	0.21	0.60	0.86	1.43	14.35
1600	100	3.1	0.17	0.40	0.48	1.20	21.34
2500	5	11.9	0.66	1.16	1.49	1.28	26.71
2500	100	9.9	0.55	0.45	0.89	1.98	37.27

Table 7-6. Bubble size measurement in three phase using self aspirated air

d_{32} (mm)											
Impeller speed (rpm)											
1600						2500					
Frother concentration (ppm)						Frother concentration (ppm)					
50			100			50			100		
No solid	Solid	After	No solid	Solid	After	No solid	Solid	After	No solid	Solid	After
0.65	0.63	0.45	0.50	0.39	0.58	0.82	0.88	0.61	0.60	0.57	0.76

Table 7-7. Bubble size measurement in two phase using forced air

Impeller (rpm)	Frother (ppm)	Q_g (L/min)	J_g (cm/s)	d_{10} (mm)	d_{32} (mm)	d_{32}/d_{10}	S_b (s^{-1})
2500	50	2.5	0.14	0.35	0.39	1.11	21.35
2500	50	5	0.28	0.41	0.45	1.10	37.01
2500	50	10	0.56	0.49	0.70	1.43	47.59
2500	50	15	0.83	0.52	0.82	1.58	60.93
2500	50	20	1.11	0.53	0.85	1.60	78.38
1600	50	2.5	0.14	0.37	0.43	1.62	19.37
1600	50	5	0.28	0.45	0.65	1.44	25.62
1600	50	10	0.56	0.52	0.89	1.71	37.43
1600	50	15	0.83	0.53	0.91	1.72	54.91
1600	50	20	1.11	0.69	1.08	1.57	61.69